Universidad Tecnológica de Pereira
Maestría en Ingeniería Eléctrica
Pereira, August 27, 2019

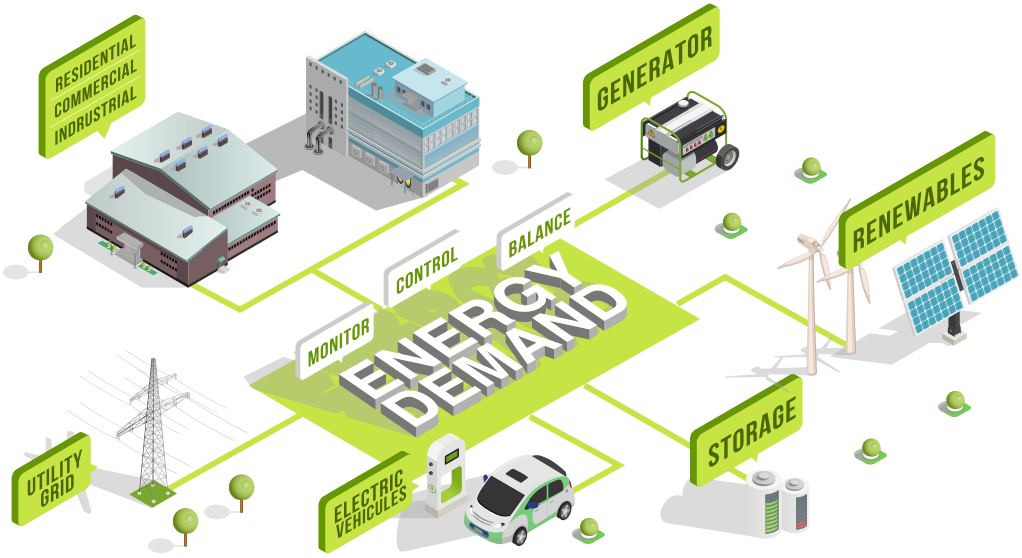

STABILITY ANALYSIS ON THE PRIMARY CONTROL IN ISLANDED AC MICROGRIDS

Master thesis presented as partial requirement for the title of Master in Electrical Engineering

By:
Manuel Fernando Bravo Lopéz

STABILITY ANALYSIS ON THE PRIMARY CONTROL IN ISLANDED AC MICROGRIDS

Manuel Fernando Bravo Lopéz

Thesis presented as a partial requirement
to qualify for the Master's Degree
in Electrical Engineering

Pereira, August 27, 2019
UNIVERSIDAD TECNOLÓGICA DE PEREIRA
Master's Program in Electrical Engineering.

STABILITY ANALYSIS ON THE PRIMARY CONTROL IN ISLANDED AC MICROGRIDS

Supervisor: Alejandro Garcés Ruiz
Co-supervisor: Walter Julián Gil

Pereira, August 27, 2019
Maestría en Ingeniería Eléctrica.
Universidad Tecnológica de Pereira
La Julita. Pereira(Colombia)
TEL: (+57)(6)3137122
www.utp.edu.co

Dedicado a
mis Padres.

Agradecimientos

El primer agradecimiento es para mí tutor el Profesor Alejandro Garcés de la Universidad Tecnológica de Pereira, por compartir su gran conocimiento, por sus sugerencias, críticas, observaciones y por todas las oportunidades que me ha brindado durante el desarrollo de este trabajo.

Muchísimas gracias a mi Madre y a mi Padre por el incondicional apoyo en el desarrollo de mi carrera profesional, también gracias a Nubia por ayudar a hacer este proceso mucho más agradable.

A todos mis amigos, gracias por compartir conmigo las experiencias más importantes de mi vida.

Un sincero agradecimiento a todos.

Funding

This thesis, is part of the research work at the ICE3 group at the Universidad Tecnolgica de Pereira (UTP). This specific research result is funded by UTP and the Colombian Administrative Department of Science, Technology and Innovation, COLCIENCIAS, project 111077657914, contract number 032-2018.

Resumen

Esta tesis presenta un nuevo modelo y análisis de estabilidad en micro-redes ac equipadas con control primario. Un modelamiento en el marco de referencia $dq0$ es propuesto para la operación de la red en forma interconectada. Un método de punto fijo es propuesto para encontrar el punto de equilibrio. Este método es a su vez comparado con un modelamiento fasorial entregando resultados cercanos. La operación en modo isla es tambien estudiada mediante una homotopía, partiendo del modo conectado. La aplicabilidad de las metodologías propuestas es demostrada usando una variante del sistema de prueba de CIGRE para aplicaciones de baja tension.

Abstract

This thesis presents a new modelling and stability analysis for ac microgrids equipped with primary control. A complete model in the reference frame $dq0$ is presented for grid connected operation. A fixed point algorithm is proposed to find the equilibrium point. This method is compared to a Newton's algorithm over the conventional phasor model. An homotopy method is proposed for the analysis of islanded microgrids. Simulations in Matlab/Simulink demonstrate the applicability of the proposed methods using a variant of the CIGRE low voltage test system.

Table of Contents

Chapter 1

Introduction

1.1 Motivation

Renewable energies and storage devices are key technologies for the Colombian case, due to the necessity of diversification of the energy mix, in the national transmission system (NTS), and the requirements of affordable and reliable generation in the non-interconnected zones (NIZ). In both cases, the aforementioned technologies require to be integrated under the concept of microgrid in order to guarantee high efficiency and reliability. New methods for stability analysis are also required, considering both the grid connected (for the NTS) and the islanded operation (for the NIZ). The later is particularly challenging due to the lack of a stiff network that maintains a constant voltage and frequency. In that case, the microgrid is responsabile for supplying its own auxiliary services including primary control of frequency and voltage.

Different control strategies have been proposed for the primary control of ac microgrids [1]. Most of these strategies are designed for ad-hoc configurations and require fast communications among devices [2]. Nevertheless, the most general and practical solution is the conventional droop used on the automatic generation control [3]. This type of control has the following advantages: i) it can be implemented in synchronous machines as well as in power electronic converters, ii) the control requires only local information, and hence, it does not require communications among devices, iii) is a simple control that does not require integral windup as is the case of PI controls.

Despite its simple implementation, the analysis of the primary control in ac microgrids is

challenging due to the nonlinear behaviour of the power electronic converters. In addition, the analysis must include the internal dynamics of the converters and their interactions. Therefore, a precise but simple model of the microgrid is required.

1.2 Problem Description

The threat represented by the climate change and the volatility of the fuel prices have encouraged the transformation of the conventional electric systems into the concept of microgrid, that is, a grid of low or medium voltage which can operate either interconnected or isolated from the main grid. Microgrids integrate efficiently non-conventional renewable sources, storage elements, controllers, communications and local consumers. Most of these technologies work on dc, therefore a power converter is needed in order to be added to the conventional ac grid.

Although the usage of microgrids is emerging in Colombia, it represents an opportunity for diversification of the energy mix and a possible modification of consumption habits. Currently, the scientific research has faced challenges regarding of the operation and control of microgrids, aimed to guarantee the optimal and safe operation of each component and caring about constrains of security in case of communications faults, grid protection in case of electric faults, the interconnection between the components from different nature and the high power variability.

The classic control of a microgrid has a hierarchical structure with three levels that are similar to the structure of the conventional electric power systems. In the lower layer, the primary control is in charge of regulating the system frequency and voltage. In a medium level, the secondary control distributes the load among generation and distributed storage devices. Finally, at the top level the tertiary control optimizes the flow with the main grid.

In the mode of connection to the grid, the system frequency and voltage do not represent a drawback for the microgrid, since these variables come fixed by the main grid. Hence, it is more challenging studying the control of the microgrid when commutes for islanded mode where power has to be provided to the critical loads and the primary control system has to manage the frequency and voltage autonomously. The control of these two variables turns out to be a non-lineal problem, thus the analysis is complex. With this in mind, the next research question comes up: ***How to analyse the stability of the primary control on islanded microgrids regarding the unbalance and the non-linearity of the sys-***

tem?

Solving this query is quite difficult since intrinsic properties of the system have to be considered such as bidirectional flows, low inertia, complex grid topology and generation uncertainty among others, which bring as a consequence the fact the most important variables of the system (frequency and voltage) might be out of the allowed operational limits.

1.3 Study Objectives

1.3.1 General

To analyze the stability of the primary control of ac microgrids operating on islanded mode, including a simplified but general model of the dynamical system in order to define conditions for the suitable operation of the grid.

1.3.2 Specifics

- To study the classic models of the primary control in ac microgrids.
- To propose a generalized model of the ac microgrid.
- To stablish a methodology for finding the equilibrium point of the ac microgrid.
- To analyze stability using the small signal theory.

1.4 Theoretical Framework

1.4.1 General Definitions

It is required previous knowledge at different engineering branches to control and operate an ac microgrid. Hereafter, it is presented some basic definitions associated with the components show in Figure 1.1.

Distributed Generation (DG)

This is a concept generally related to microgrids that consists of electric generation in a small scale, whose main resources are commonly renewable (solar, wind, thermal, etc.), with

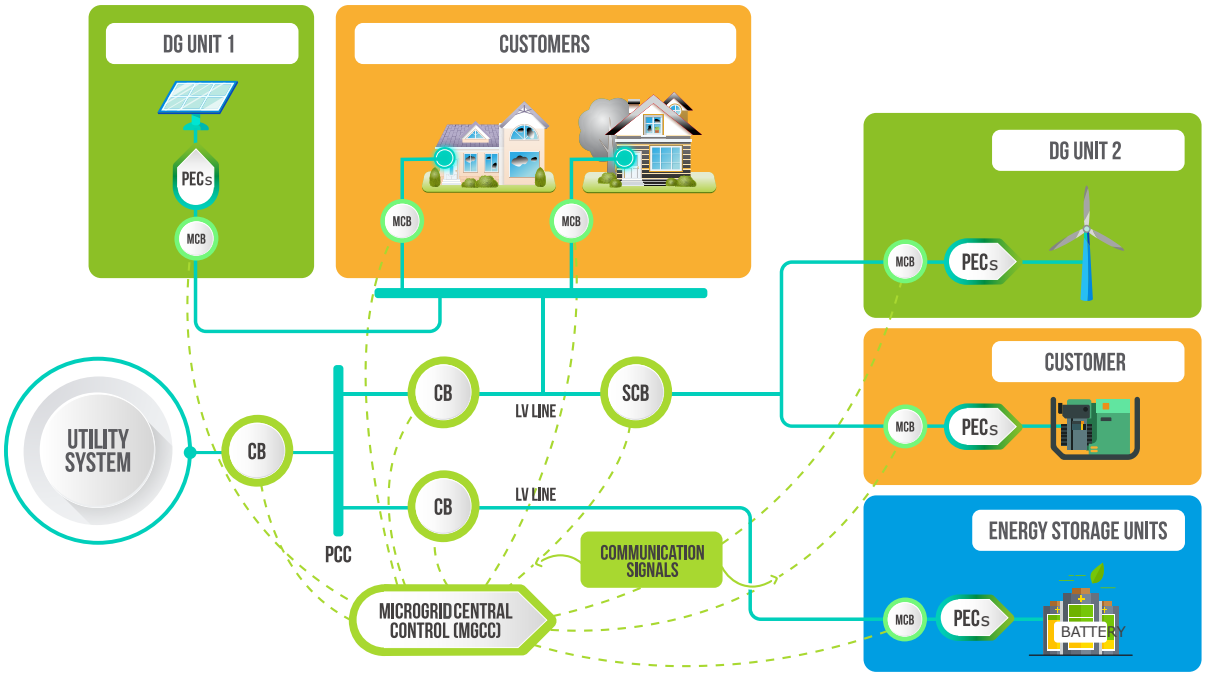

Figure 1.1: AC Microgrid Components [4]

a particular characteristic with regards to the location as components are close to the loads or consumers [5].

Microgrid (MG)

A microgrid is an "agregation" of loads and microsources of generation, which work as a unique system and provides energy and heat. Most of the microsources must be based on power electronics to provide the necessary flexibility in order to work as a unique aggregated power system. This flexibility of control allows to be represented as a unified controlled unit which satisfies the local needs of reliability and security [6]. This concept differs from the previous one, in the way as the components are aggregated including communications among units of generation and capability of isolated operation in case of problems coming up in the grid. This should have autonomy in the matter of connection and disconnection, which is not possible with the DG where the component has to be disconnected automatically in this situation.

Communication systems

The communication systems play and very important role, since they are in charge of supervising the microgrid converters through the bidirectional flow of information which contains generally voltages, power flow, load connection and disconnection. The communication networks for MGs are classified according to the coverage area. Some types are the Home Area Networks (HAN), the Neighborhood Area Network (NAN) and the Wide Area Network (WAN) [7].

Control systems

The success of the communications is highly related to the control structure and scheme of the MG, in some international scientific literature articles are classified in two groups. The first one include active techniques of which in turns are subclasified into four types: centered control, master-slave, ring structure and average load delivery; the second group has the droop schemes [8]. Hereafter, some of them are described:

- Centered control (Master-slave): In the case of the centered scheme (see Figure 1.1), a central controller is used to regulate the action of the elements of the network with the aim of keeping the balance of active and reactive power [9].
- Ring structure: in this control strategy the power distribution has a circular trajectory among the converters, Its require a communication scheme of bidirectional data, which will allow to have exchangeable modules on real time [10].
- Droop control: For the droop schemes its not needed a complex communication system (not a critical communications systems) among the parallel connected modules, since each module sets its phase and voltage reference according to the load (active power and consumed reactive power) [11]. This scheme of control is show in Figure 1.2.

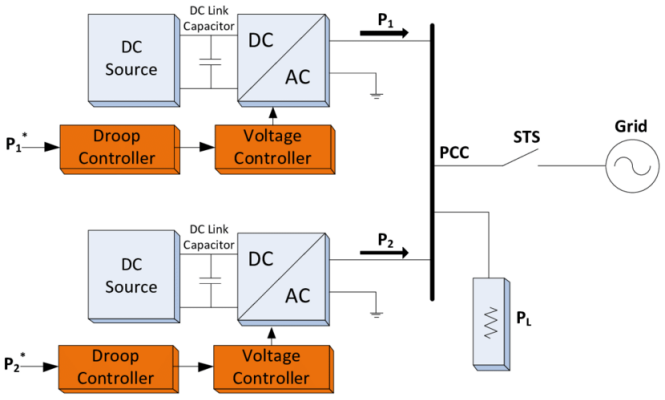

Figure 1.2: Microgrid and their voltage and droop control [12]

Power converter

They are in charge of transforming the electric energy coming from the small generators from the renewable energies (for instance, photovoltaic energy), storage (batteries, capacitors, flywheels) and controllable loads. Only forced-commutated converters are considered since these allow complete controllability of active and reactive power.

1.5 State of the Art

Modelling

This work is intended to embrace the analysis of the stability of the microgrids which rely on a strategy of primary control operating on an isolated mode, looking for conditions which guarantee stability and proper operation of the system. Inside this research topic some works have been carried out in the Universidad Tecnológica de Pereira and other Colombian universities; where different strategies of control, topology for controlling converters, component developments for synchronizing the microgrids with the main grid and others are analyzed, which are helpful to solve in a minor way the problems triggered by this new grid concept [13].

Currently, in the international literature it can be found several microgrid models, most of them designed for small signals stability analysis through the representation in state of spaces [14]. Other authors propose models based on the admittance to carry out the stability analysis using the Routh-Hurwitz stability criteria, where the stability conditions are

provided in terms of physical parameters of the system, such as the one proposed in [15]. Some authors propose other kind of models based on phasor representations of the MGs, for instance the one proposed in [16] named Impedance matching based stability criteria for ac microgrids.

A very remarkable aspect in the microgrid modelling and which is independent from the type of model used for the stability model, as well the grid operation mode, has to do with the reference framework in which it is developed the model of each one of the elements of the microgrid. In [14], [15] and [17], the authors propose different stability analysis with a common matter which is the system modelling is developed in the 0-d-q framework. These show a clear reference point to start the modelling stage required by the research.

Stability Analysis

The stability can be defined as the capability of the system to stay in balance after the system has suffered a disturbance. These disturbances might affect the system stability in multiple ways, therefore the literature has proposed classifications for analyzing the stability of electric power systems. In [18] it is proposed a detailed classification taking into account the disturbed variable in the power system, the magnitude of the disturbance and the time frame should be considered to analyze the stability problem.

Due to the implicit properties of the microgrids and the existing differences from the conventional power systems, the stability has to be analyzed from a different perspective [19]. Some authors have contributed with the microgrids stability classification, in [19] and [20] it can be found works about the microgrids stability in three classes, namely: 1) Small signal stability, 2) Transient stability, and 3) Voltage stability.

The small signal stability is related to the small disturbances due to small changes on the load, capability power limits of generation sources, system storage and weakness on control systems. In [21] and [22], the authors show the analysis of small signal on microgrids based on the linearization of the model close to an operation point.

Regarding the transient stability in [23], the authors carry out a classification of the state of the art according to the operation mode of the microgrid which shown a general focus on the study of big disturbances, type of faults and big changes on the charge, to analyze this type of stability non-linear models are used with techniques such as Lyapunov functions.

With regards to the voltage stability in the literature it can be noticed it is associated with the limits of reactive power, dynamic charge and changes on the transformers taps [19].

1.6 Contributions

The main contributions of this thesis are presented in the following three items:

- **Modelling:** a complete dynamic model for three-phase microgrids and smart distribution systems is studied and all the components are modelled in a $dq0$ reference frame. A simplified model of the power electronic converters is proposed using the Akagui/Aredes power theory and is compared to a complete vector oriented control model.
- **Equilibrium point:** The contribution of this step is related with the algorithm for solving the equilibrium point in the $dq0$ reference frame on the CIGRE microgrid system. In this thesis the connected and islanded equilibrium point is found. For both operation modes this point is found using a fixed point iteration similar to the Gauss method. Based in the connected operation mode is proposed a strategy to find the islanded equilibrium point.
- **Stability analysis:** A stability analysis is accomplished over a complete islanded microgrid system (loads, converters, lines) are include, the results show a stable microgrid around of the stable state point al least in small signal, under a select the values of the active and reactive power delivers by the converters. This is achieved by small signal stability theory.

1.6.1 Research results

- Authors: Manuel Bravo, Alejandro Garcés, Oscar D. Montoya, Carlos R. Baier. Title: Non-linear Analysis for the Three-Phase PLL: A New Look for a Classical Problem. Presented in 2018 IEEE 19th Workshop on Control and Modeling for Power Electronics (COMPEL), June 25, 2018, Padova, Italy.
- Authors: Manuel-Fernando Bravo, Alejandro Garcés, Sandra Pérez-Londoño. Title: Power Flow in Islanded Microgrids: Formulation and Convergence Analysis. Acepted in IEEE PES General Meeting 2019, August 4-8, 2019, Atlanta, GA, USA.
- Authors: Manuel Bravo-López, Alejandro Garcés, J. Mora-Flórez. Analysis of Microgrids on the 0dq Reference Frame: Dynamical Model, Equilibrium Point and Averaging. Submitted to Electric Power System Research.

1.7 Structure of the Thesis

The objective of this thesis is to perform a stability analysis to an islanded ac microgrid. This includes performing processes such as: modelling the of microgrid elements finding the point of steady state as is mentioned in section 1.6. Chapter 3 presents a complete dynamical model of the grid. It starts by a three-phase modeling in the reference frame abc which is transformed by using the invariant Parks transformation in order to obtain a compact representation on the $dq0$ reference frame; a simplified model of the power electronic converters is also presented in this section. Next, two algorithms for finding the equilibrium point are developed in Chapter 4 [1]. This algorithms has different approaches but fulfill the same function of find the islanded equilibrium point of a test system. Furthermore, the algorithm that comprises the more detailed grid model is submitted to a stability analysis based on eigenvalue analysis, this is explained in Chapter 5. Finally the test system parameters of CIGRE benchmark low voltage microgrid and the mathematical background are presented in Appendix A.

For better understanding, the structure of this thesis is shown in Figure 1.3. Each chapter is depicted by a rectangle containing the main features of it, the next chapter will involve the conclusions of the previous chapter. For instance, Chapter 2 contains the converter model that is used to complete the microgrid model proposed in Chapter 3, in the following chapter the resulting complete microgrid model is used to find the equilibrium point based in two proposed algorithms and finally in Chapter 5 the equilibrium found is used to linearize the system and to perform the stability analysis.

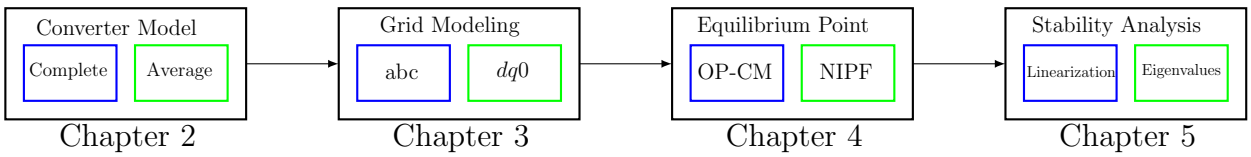

Figure 1.3: Structure of the thesis

[1] The terms NIPF and OP-CM are used in chapter 4 to refers two proposed algorithms that allow to obtain the islanded microgrid equilibrium point, so called Islanded Newton Power Flow and Optimization and Contraction Mapping methods, respectively.

Chapter 2

Model of the converter

2.1 The voltage source converter

One of the most important elements in microgrids is known as a power electronic converter and is in charge for integrating distributed generation sources and local loads into the system. Therefore, studying this element is very useful for subsequent analyzes associated with the microgrid operation. The conventional scheme of a VSC comprises the set of semiconductors switches like gate-turn-off thyristors (GTOs), insulated gate bipolar transistors (IGBTs), or gate controlled thyristors (IGCTs) organized in three legs (depending on the nature of the system to which it is going to connect). This switches receives the control signals (pulses), coming from the pulse width modulator (PWM) to produce a controlled dc voltage and convert of one type of current to another, for instance (dc - ac) as is show in Figure 2.1.

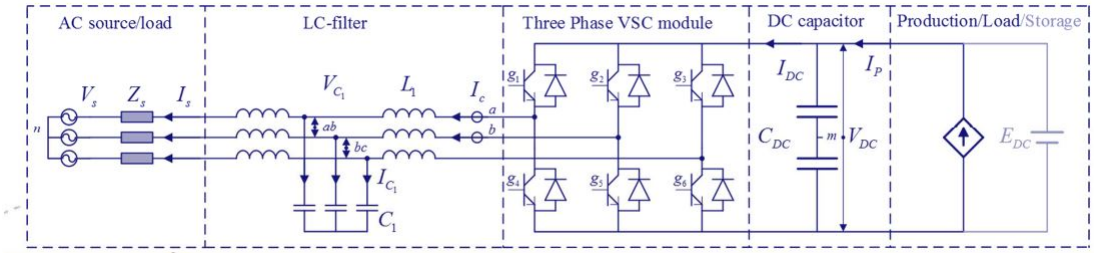

Figure 2.1: Three-phase VSC connection to the main grid scheme [24]

For the three-phase case the switches are drives by a sequence function that alternatively

Table 2.1: Sumary of operation modes of power electronic converters [27]

Converter	Representation	Attributes
Grid Following	Current source	Deliver power references to an energized grid Should be perfectly synchronized No islanded mode (additional power converter manage f and $\|V\|$) Operate by high level controller Requires PLL
Grid Forming	Voltage source	Setting the references voltage amplitude $\|V\|$ and frequency f Should be perfectly synchronized in parallel operation with others converters Islanded mode Requires PLL to grid connection
Grid Supporting	Current source Voltage source	Regulate the grid frequency f and voltage amplitude $\|V\|$ If is a current source it need at least one grid forming converter Is in between grid forming and grid following Deliver active an reactive power to keep the values of f and $\|V\|$ Voltage source operate in both modes

switch the g1 and g4 semiconductors of the first leg, g2 and g4 of the second leg and g3 and g6 of the third leg, which successively connect the terminals a, b and c of the inverter with the dc side of the generation source, the result of this process is a square voltage wave between the dc voltage levels $+V_{dc}$ 0 $-V_{dc}$ [25]. On the other hand, to control efficiently the switch switching is required measure some variables such as dc voltage (dc link), ac outputs voltage and currents, as is show in Figure 2.1. In all the block diagrams of this document the variables are found in per unit and in addition those that are accompanied by * represent reference values.

This signals are send to the control system that consists of a series of blocks connected in cascade that modify the pulses that receive the IGBTs for example, to control the voltage of the dc side or the active power and the reactive power that can be injected to the main grid by the generation source.

With respect to operation mode of power electronic converters, three types were identified, namely: grid forming, grid following and grid supporting [27]. Each one is based on the designated control objectives into the microgrid. Table 2.1 shows a summary, that allows identify the best solution according to the microgrid needs.

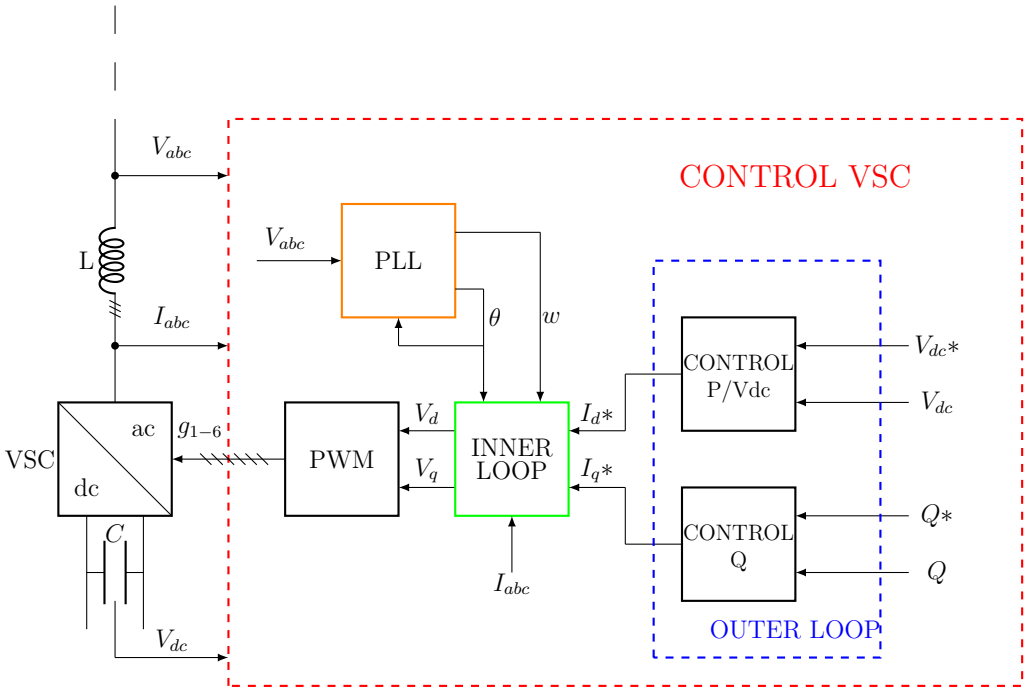

Figure 2.2: Control scheme for the grid conected VSC [26]. *Note: In all the block diagrams of this document the variables are found in per unit and in addition those that are accompanied by * represent reference values.*

2.2 Voltage oriented control

In the literature, a variety of techniques to control a VSC has been presented, such as voltage oriented control (VOC), resonant current controllers (RCC), hysteresis current controllers (HCC) and model-based predictive control (MPC) [28], each one of these techniques has an advantages which depend of the application. For the propose of this thesis the VOC is the studied, since it is the most common strategy in the industry.

As mentioned before, the control system is composed by a set of blocks that receives and process the signals to give the reference signals to the next block. To understand the control scheme of the VSC, in this section is described each one of the blocks that shape the VOC show in Figure 2.2, before starting it is necessary to remember the transformation of the coordinates theory.

2.2.1 Park transformation or $dq0$

The Park transformation performs the change of the abc three-phase components to the synchronous reference frame components $dq0$. This transformation convert the sinusoidal variables of the three-phase system to constant variables in the permanent regime. The vector of the components for the new reference system X_{dq0} is obtained by multiplying the transformation matrix $[T]$ with the vector of three-phase components X_{abc} [29], as follows:

$$\begin{pmatrix} X_d \\ X_q \\ X_0 \end{pmatrix} = \begin{pmatrix} \ T \ \end{pmatrix} \begin{pmatrix} X_a \\ X_b \\ X_c \end{pmatrix} \tag{2.1}$$

where:

$$[T] = \begin{pmatrix} cos(\theta) & cos(\theta - 2\pi/3) & cos(\theta + 2\pi/3) \\ sin(\theta) & sin(\theta - 2\pi/3) & sin(\theta + 2\pi/3) \\ 1/2 & 1/2 & 1/2 \end{pmatrix} \tag{2.2}$$

In the same way it is possible to return the original X_{abc} components by applying Park's inverse transformation, multiplying the inverse transformation matrix $[T]^{-1}$ by the components vector X_{dq0}, as is presented in 2.3:

$$\begin{pmatrix} X_a \\ X_b \\ X_c \end{pmatrix} = [T]^{-1} \begin{pmatrix} X_d \\ X_q \\ X_0 \end{pmatrix} \tag{2.3}$$

There are different versions of the Park's transformation. In this thesis, the power invariant Park's transformation was used. This transformation has as main characteristics that $[T]^{-1} = [T]^{\top}$ meaning that the dot product is preserved. Thus, the power in both reference frames is equal.

2.2.2 Phase locked loop (PLL)

The PLL is the element that carries out the synchronization of the converter with the voltage of the main grid, to guarantee the control of the active and reactive power, since the calculation of the power in the frame of reference $dq0$ can be defined as:

$$S = p + jq = v_{dq} i^*_{dq} = (v_d + jv_q)(i_d - ji_q) = v_d i_d + v_q i_q + j(-v_d i_q + v_q i_d) \tag{2.4}$$

To synchronize the VSC with the voltage of main grid, the PLL estimates the necessary voltage angle θ to apply the $dq0$ transformation, this assuming perfect alignment of the voltage magnitude with the axis d, which entails that the component q of the voltage is equal to zero. The process is show in Figure 2.3, where the $\Delta\theta$ angle error can be calculated by the following expression:

$$\Delta\theta = \tan^{-1}\left(\frac{v_q}{v_d}\right) \tag{2.5}$$

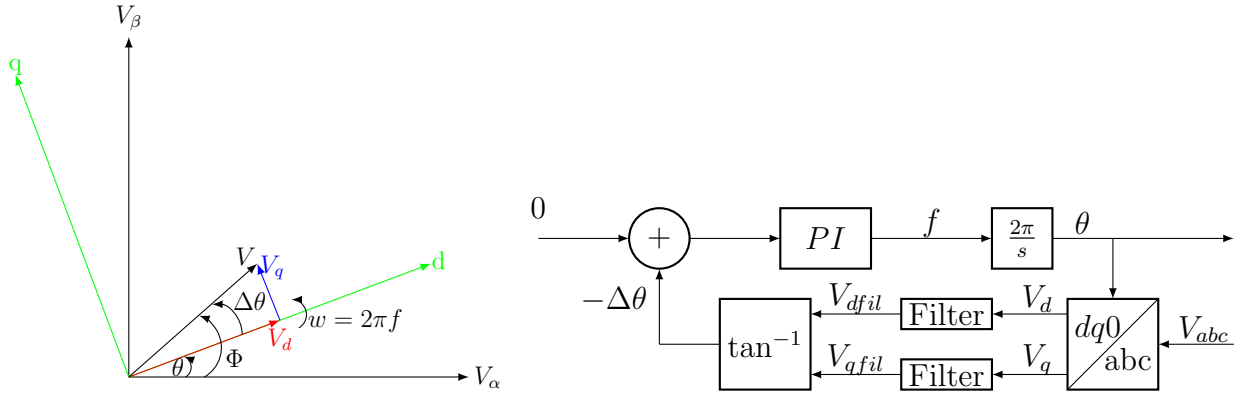

(a) PLL estimation angle θ (b) PLL blocks diagram

Figure 2.3: Three-phase PLL phase angle estimation and control diagrams [30]

In the international literature a variety of PLL models are proposed, were the control scheme depends on such aspects as the phase number in the system and the reference variables, for example. For this thesis study case, it is necessary a three-phase PLL were the phase angle error was taken as a reference. The control scheme responds to the block diagram in Figure 2.3b.

The input variables on the PLL block diagram show in Figure 2.3b are the measured three-phase grid voltages V_{abc} and using the Park's transformation are obtain the magnitude voltages in the $dq0$ reference frame V_{dq0}. To eliminate the signal noise this transformed measures are pass through a low pass filter, the next process comprises compute the $\Delta\theta$ and

control the value using a classical PI controller. The PLL outputs are the electrical grid frequency f and the voltage angle θ.

2.2.3 Current control (inner-loop)

The next stage in the VOC is known as inner-loop, that is responsible of controlling the output converter currents by controlling the output voltage, the development of this control loop is made by the set converter-filter-grid modelling [31]. A VSC connected to an ac grid can operate as a synchronous motor/ generator with the characteristic that its inertia is low. Then, in the same way to a synchronous machine, the converter can manage the active and reactive power flow, as shown in Figure 2.4 [32], where V_s is the fundamental component of the voltage generated by the VSC and V_{grid} is the fundamental component of the ac grid voltage.

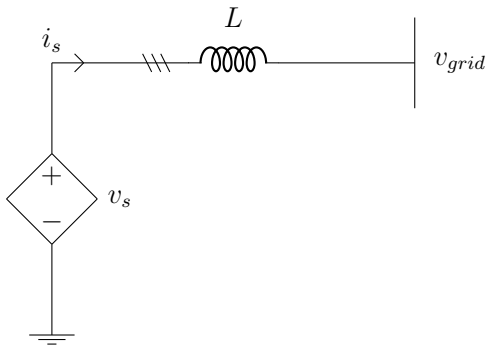

Figure 2.4: Equivalent circuit of three-phase grid connected VSC

The abc reference model of the electrical diagram presented in Figure 2.4, has the following structure:

$$V_s = L\frac{dI_s}{dt} + V_{red} \tag{2.6}$$

Note from Figure 2.3a that:

$$V_{\alpha\beta} = Ve^{j\Phi} \tag{2.7}$$
$$V_{dq} = Ve^{j\Delta\theta} \tag{2.8}$$
$$\theta = wt \tag{2.9}$$

So that:

$$V_{dq} = Ve^{j(\Phi-\theta)} \tag{2.10}$$
$$V_{dq} = Ve^{j\Phi}e^{-j\theta} \tag{2.11}$$
$$V_{dq}e^{j\theta} = Ve^{j\Phi} \tag{2.12}$$
$$V_{\alpha\beta} = V_{dq}e^{j\theta} \tag{2.13}$$

Presenting (2.6) in $\alpha\beta$ coordinates and multiplying in both sides by $e^{-j\theta}$, is obtained (2.14) and (2.15):

$$V_{s_{\alpha\beta}} = L\frac{dI_{s_{\alpha\beta}}}{dt} + V_{red_{\alpha\beta}} \tag{2.14}$$
$$V_{s_{\alpha\beta}}e^{-j\theta} = Le^{-j\theta}\frac{dI_{s_{\alpha\beta}}}{dt} + V_{red_{\alpha\beta}}e^{-j\theta} \tag{2.15}$$

By replacing (2.13) in (2.15), it is possible obtain the following expression:

$$V_{s_{dq}} = Le^{-j\theta}\frac{dI_{s_{\alpha\beta}}}{dt} + V_{red_{dq}} \tag{2.16}$$

Where it is possible to show that $e^{-j\theta}\frac{dI_{s_{\alpha\beta}}}{dt}$ is equal to:

$$e^{-j\theta}\frac{dI_{s_{\alpha\beta}}}{dt} = \frac{dI_{s_{dq}}}{dt} + jwI_{s_{dq}} \tag{2.17}$$

By replacing (2.17) in (2.16), the dq representation of the system in Figure.2.4 is finally obtained:

$$V_{s_{dq}} = L\frac{dI_{s_{dq}}}{dt} + jwLI_{s_{dq}} + V_{red_{dq}} \tag{2.18}$$

Decomposing (2.18) on its two components d and q, it is possible to notice that the voltage at the output of the converter can be controlled like this:

$$V_{s_d} = L\frac{dI_{s_d}}{dt} - wLI_{s_q} + V_{red_d} \tag{2.19}$$

$$V_{s_q} = L\frac{dI_{s_q}}{dt} + wLI_{s_d} + V_{red_q} \tag{2.20}$$

In (2.19) and (2.20), there is a term that presents conflict since in each equation exist a variable that depends of the other control variable, to eliminate this problem it is enough to define two variables that eliminate these crossed terms, as presented in (2.21) and (2.22) :

$$u_d = V_{s_d} + wLI_{s_q} \tag{2.21}$$

$$u_q = V_{s_q} - wLI_{s_d} \tag{2.22}$$

Replacing (2.19) in (2.21) and (2.20) in (2.22)), the new variables take the following form:

$$u_d = L\frac{dI_{s_d}}{dt} + V_{red_d} \tag{2.23}$$

$$u_q = L\frac{dI_{s_q}}{dt} + V_{red_q} \tag{2.24}$$

Already at this point it is possible to define the control scheme for the voltage at the output of the converter represented in Figure 2.2 as inner-loop. The block diagram that represents this control has the following structure:

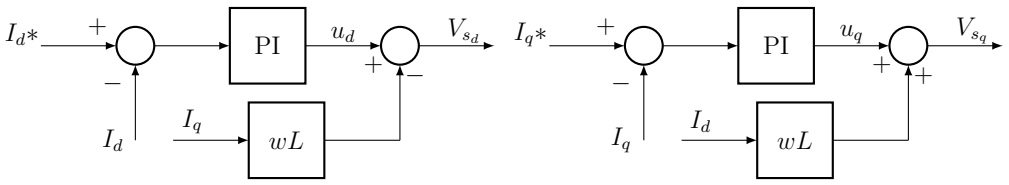

(a) Control inner-loop axis d (b) Control inner-loop axis q

Figure 2.5: Inner-loop control scheme

The block diagram in Figure 2.5 show that it receives as inputs the reference currents I_d* and I_q*, the sensed currents at the output of the converter are after passing through a block that transforms them into the $dq0$ reference frame by means of the Park transform, the frequency and the phase angle are estimated by the PLL.

2.2.4 Active (P) / dc voltage (V_{dc}) and Reactive (Q) power controls (outer-loop)

The outer-loop assigns the direct and quadrature reference currents for the inner-loop. The function of this block is to management the active and reactive power that is desired at the output of the converter in one of the cases or in the management of the dc voltage of the converter instead of the active power. The block for the control of the active power P or the voltage of the dc side has the same structure as that of the block for the control of reactive power Q, the only variant is related to the variables to be controlled and the output variables. Such a structure is shown in Figure 2.6 [33].

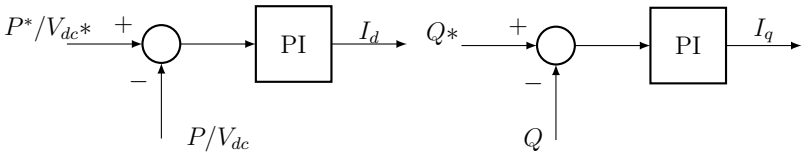

(a) Control outer-loop P/V_{dc} (b) Control outer-loop Q

Figure 2.6: Outer-loop control scheme

The control objectives of these blocks are achieved following the equation (2.4) and some considerations in the system, among them it is assumed that the converter is ideal that is to say there are no losses in the electronic components, so the power on the ac P_{ac} side is equal to the power that is transferred from the dc P_{dc} side or in the opposite direction. The PLL is able to estimate the nominal values of the system and that V_d of steady state is close to 1 in pu, that is:

$$P_{ac} = P_{dc} \tag{2.25}$$

$$V_q = 0 \tag{2.26}$$

$$V_d = 1 \tag{2.27}$$

Recalling equation (2.4), if the real part of this expression is taken and it is assumed that the dc voltage is managed by an earlier stage it is possible to notice the relationship that exists between the active power P_{ac} and the direct axis current I_d, as is present in the following equations:

$$P_{ac} = v_d i_d + v_q i_q \tag{2.28}$$
$$P_{ac} = i_d \tag{2.29}$$

On the other hand, when the control objective is the voltage on the dc side, only is necessary make a change of variables between measures variables of active power and dc voltage, also is necessary a change on the reference values if the magnitude of these variables are not in pu, the dependence demonstration of V_{dc} variable with the direct axis current is derived from consider that the system has no losses and the relationship between the dc side and the ac side, through the following equations:

$$I_{fuente} = C\frac{dV_{dc}}{dt} + I_{dc} \tag{2.30}$$
$$V_{dc} I_{dc} = V_d I_d \tag{2.31}$$

When it is desired to control the reactive power Q the relation of this variable with the current of quadrature axis i_q, the action is similar to the active power control and its foundation is limited to taking the imaginary part of (2.4), as is present in (2.32) and using the consideration that V_d are equal to 1 pu the relation is demonstrated in (2.33):

$$Q_{ac} = -v_d i_q + v_q i_d \tag{2.32}$$
$$Q_{ac} = -i_q \tag{2.33}$$

2.2.5 Pulse width modulation (PWM)

To finish with the detailed presentation of VOC technique, the PWM block are not specified in detail, since in the implementation for this thesis work it was not used. The inverter model used is based on the averaged model where the inputs are the three-phase reference voltages instead of the signal pulses from the PWM.

2.3 Primary control in microgrids

With the microgrids integration to the power systems, a series of properties are aggregated to this systems. This is the case of islanded operation, where a part of the electrical power system can be operates as a total independent entity, other relevant aspect is the power sharing between the parallel converters and also with the main grid. This characteristics requires a rigorous monitoring of some variables on the electric power system to ensure the stable and efficient operation. The more representatives variables are the voltage $|V|$ and the frequency f. To control these variables the use of primary control is the most common used technique [27].

It is important analyse the behaviour of this variables, because this work focuses in the islanded operation of migrogrids, where is necessary take into account some aspects such as: 1) The absence of reference or slack bus which is able to maintain bus voltage and f constants, 2) The frequency variation due to power imbalances. Thus when the microgrid operate in islanded mode the power converters that incorporate the distributed generators (DG) units must have an scheme of primary control, based in a frequency/active power (f/P) and voltage/reactive power (V/Q) droop control. Since this technique operates in local way and the use of communication systems is not necessary.

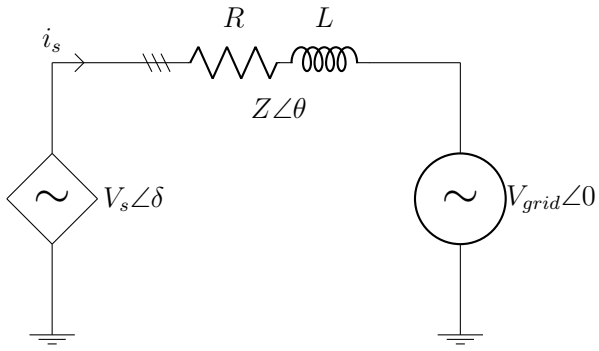

Figure 2.7: Simplified modeling of power converter connected to a distribution network equivalent circuit.

To understand the aforementioned relation, it is necessary to consider the power flow through a line impedance that interconnect a power electronic converter modelled as an ideal controllable voltage source and a voltage source that modelled the main grid, as shown in Figure 2.7. The model of this system is described by the following equations:

$$S = V_{grid} I^* \tag{2.34}$$

$$S = \frac{|V_{grid}||V_s|\angle\theta - \delta}{|Z|} - \frac{|V_{grid}|^2\angle\theta}{|Z|} \tag{2.35}$$

With $Z = R + jX$ and taking the real and imaginary parts of (2.35), the active and reactive power flow general expressions are obtained:

$$P = \frac{|V_{grid}||V_s|\cos(\theta - \delta)}{|Z|} - \frac{|V_{grid}|^2\cos(\theta)}{|Z|} \tag{2.36}$$

$$Q = \frac{|V_{grid}||V_s|\sin(\theta - \delta)}{|Z|} - \frac{|V_{grid}|^2\sin(\theta)}{|Z|} \tag{2.37}$$

From (2.36) and (2.37) is possible demonstrate the relation (w/P) and (V/Q) for pure inductive line case, how is the case for high voltage (HV) and medium voltage (MV) power systems, this is equivalent to neglected the resistive part of Z, so $\theta = 90$. Additionally in this line types, the power angle δ is small, so it entails that $\sin(\delta) \approx \delta$ and $\cos(\delta) \approx 1$, so that the relation is defined by (2.38) and (2.39).

$$P = \frac{|V_{grid}||V_s|}{|Z|}\delta \tag{2.38}$$

$$Q = \frac{|V_{grid}||V_s| - |V_{grid}|^2}{|Z|} \tag{2.39}$$

These relationships permit to control the grid frequency and voltage at the common point of connection, by change the reference value of the active and reactive powers delivered by the converter, respectively. The control structure for both variables are defined by the following equations:

$$f - f_{ref} = -K_P(P - P_{ref}) \tag{2.40}$$

$$V - V_{ref} = -K_Q(Q - Q_{ref}) \tag{2.41}$$

where $f - f_{ref}$ and $V - V_{ref}$ are the grid frequency and voltage deviations, and $P - P_{ref}$ and $Q - Q_{ref}$ are the necessary variations in the active and reactive power injected by the

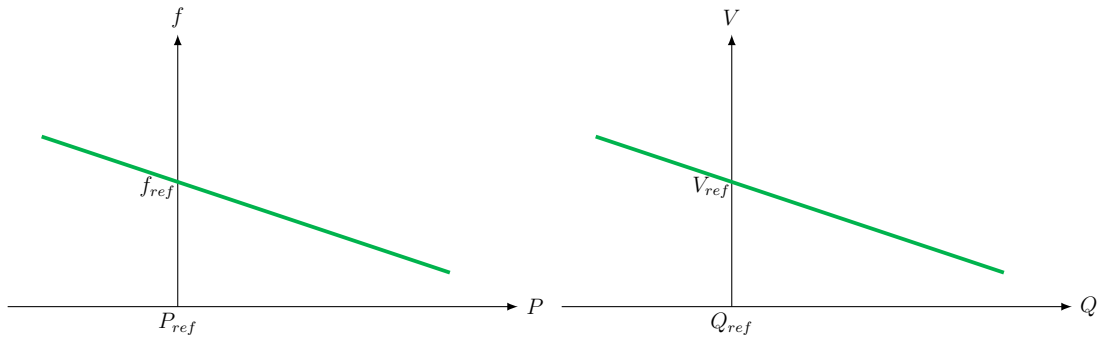

Figure 2.8: Nodal active and reactive injected power by a)Converter with P/f droop control b)Converter with Q/V droop control, inductive case.

converter, respectively, to manage the system variables and carry to their rated values, and K_P and K_Q are the droop control gains. Graphically this relation is shown in Figure 2.8

On the other hand, is important to notice that these relations are inverse when the transmission line is in a low voltage (LV) power system. The demonstration is similar to the inductive case, only the next change in the considerations is make, the line impedance Z is only resistive, so the angle $\theta = 0$. With this in mind the droop control equations (2.36) and (2.37) take the following form:

$$P = \frac{|V_{grid}||V_s| - |V_{grid}|^2}{|Z|} \tag{2.42}$$

$$Q = -\frac{|V_{grid}||V_s|}{|Z|}\delta \tag{2.43}$$

It is clear from (2.42) and (2.43) the difference with the inductive line case, also the negative sign in the reactive power in the resistive case, what it entails a change in the sign in the K_Q droop control constant. So the droop control for LV case is defined by (2.44) and (2.45). The dynamics of droop control for this case are shown in Figure (2.9).

$$V - V_{ref} = -K_P(P - P_{ref}) \tag{2.44}$$
$$f - f_{ref} = K_Q(Q - Q_{ref}) \tag{2.45}$$

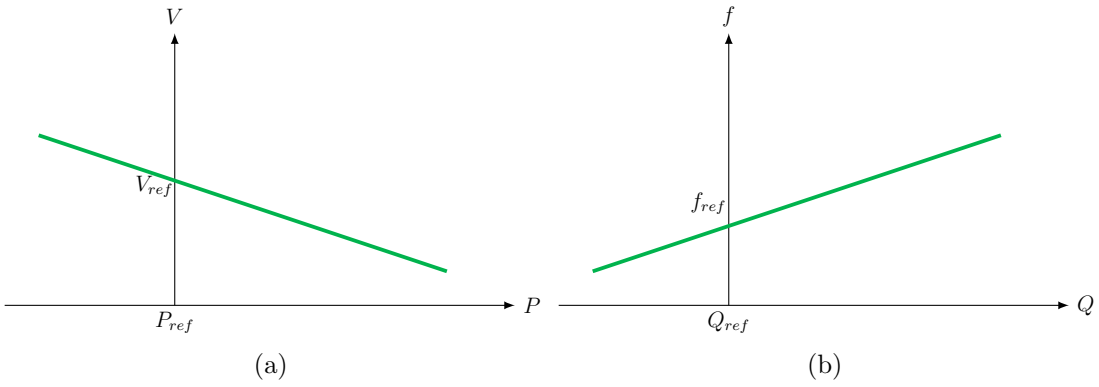

Figure 2.9: Nodal active and reactive injected power by a)Converter with P/f droop control b)Converter with Q/V droop control, resistive case.

For both cases the active and reactive powers that the converter will deliver to the grid is computed based in the block diagrams in Figure 2.10, where, f and $|V|$ are the measured frequency and nodal voltage respectively, f_{ref} and V_{ref} are the nominal angular frequency and voltage reference, P_{ref} and Q_{ref} are the amount of active power an reactive needed in each node.

2.4 Proposed simplified model

In general, each terminal is integrated through a power electronic converter which maintains a constant active and reactive power, as mentioned earlier, the most common converter for microgrid applications is the pulse-width modulated voltage source converter (VSC) and this converter can integrate different distributed resources such as solar panels, wind turbines and energy storage devices including batteries, super-magnetic energy storage and super-capacitors. The control of the converter can be obtained in different ways, but the most

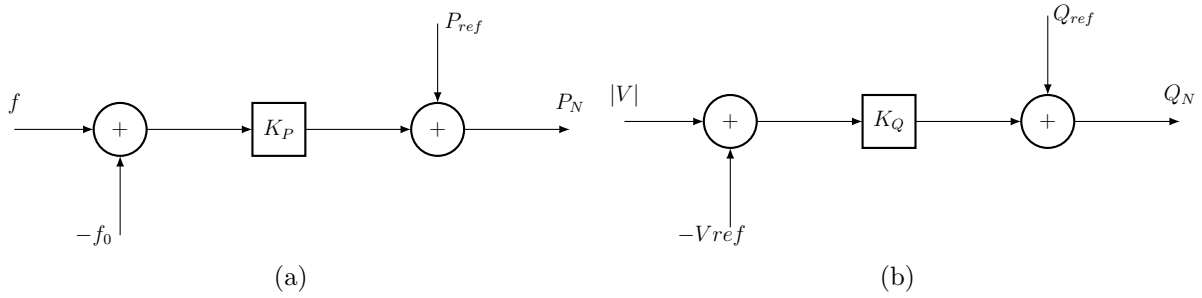

Figure 2.10: Control diagram of a)Nodal active power injected by converter with P/f droop control b)Nodal reactive power injected by converter with Q/V droop control, general structure.

common approach is the vector oriented control [34] described in this chapter and summarized in Figure 2.2.

In contradistinction to the complex VOC for the VSC, in this section a simplified converter model on $dq0$ reference frame is proposed. The zero sequence current in this simplified converter is set to zero, although a converter can inject zero sequence in the grid, it should have a fourth leg connected to the neutral point, which is an unusual configuration in industrial practice [35]. —By using the Akagui's instantaneous power theory [36], the current injected in each node by the converter is obtained as function of the active and reactive power as given in (2.46).

$$\begin{pmatrix} i_0 \\ i_d \\ i_q \end{pmatrix} = \frac{-y_P}{v_d^2 + v_q^2} \begin{pmatrix} 0 & 0 & 0 \\ 0 & 1 & 0 \\ 0 & 0 & 1 \end{pmatrix} \begin{pmatrix} v_0 \\ v_d \\ v_q \end{pmatrix} + \frac{y_Q}{v_d^2 + v_q^2} \begin{pmatrix} 0 & 0 & 0 \\ 0 & 0 & 1 \\ 0 & -1 & 0 \end{pmatrix} \begin{pmatrix} v_0 \\ v_d \\ v_q \end{pmatrix} \tag{2.46}$$

The model comprises a nodal ($\mathcal{N}$) currents vector $J_{\mathcal{N}}(x, y)$ that is built by grouping i_0, i_d, i_q in all the nodes of the grid. Step nodes can be also represented in $J_{\mathcal{N}}(x, y)$ by making $P = 0$ and $Q = 0$, thus, this representation is general enough for practical microgrids with power electronic converters. Notice from 2.46 that $J_{\mathcal{N}}(x, y)$ is a non-linear function of nodal voltages $V_{\mathcal{N}}$ and gives all the required information for the power electronic converters. The vector $J_{\mathcal{N}}$ takes therefore the structure proposed in (2.47)

$$J_{\mathcal{N}}(x,y) = m_P(x_v, y_P)x_v + m_Q(x_v, y_Q)x_v \tag{2.47}$$

where $y = (y_P, y_Q)$ are state variables from the internal control of the converters. Equation (2.47) is non-linear making the model non-linear. Notice that m_Q is skew-symmetric and $m_P \succeq 0$ if $P \geq 0$.

On the other hand, the internal dynamics of the converters can be included with any desired level of detail. In this case, a first order model that only requires the time constant associated to the delay of the control is proposed in Figure 2.11.

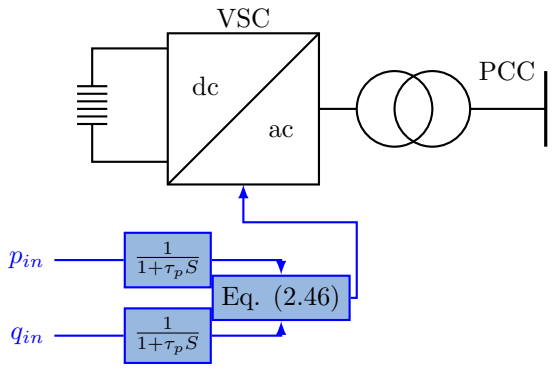

Figure 2.11: Proposed first order model for three-phase voltage source converters

Therefore, the following equations are obtained, where τ is the time constant. This model will be validated in the next section.

$$\tau_P \dot{y}_P = P - y_P \tag{2.48}$$
$$\tau_Q \dot{y}_Q = Q - y_Q \tag{2.49}$$

This model converter model can be classified into the converters that are controller in the grid supporting mode in accordance with the Table 2.1, since the control objectives in this case are inject the required power in order to set the microgrid frequency and voltage magnitude in a admissible value according to the regulation of each grid operator. On the other hand, is possible change the control objectives of the proposed reduced converter model by changing the output variables in equation 2.46, with the aim of select the best solution for the microgrid needs, for example implement a grid following converter.

2.5 Results

This section shows the performance of both converter models described above. The SIMULINK/ MATLAB implementations are also shown. A test will show the dynamic response under the same conditions. This with the purpose of compare them and get some conclusions.

Figures 2.12 and 2.13, show the diagram blocks for the control of grid connected VSC using the VOC technique, and the diagram blocks for the first order proposed converter model, respectively. In Figure 2.12 the control objectives are the dc voltage and the reactive power, remember that the control of dc voltage can be replaced by the active power using the same structure, only a change in the reference and measured values is required. In this figure the references in the active and reactive power give the reference i_d and i_q currents to the inner-loop, and it finally give the voltage references to the VSC, so get, at the converter output the programmed P and Q power to inject at the main grid.

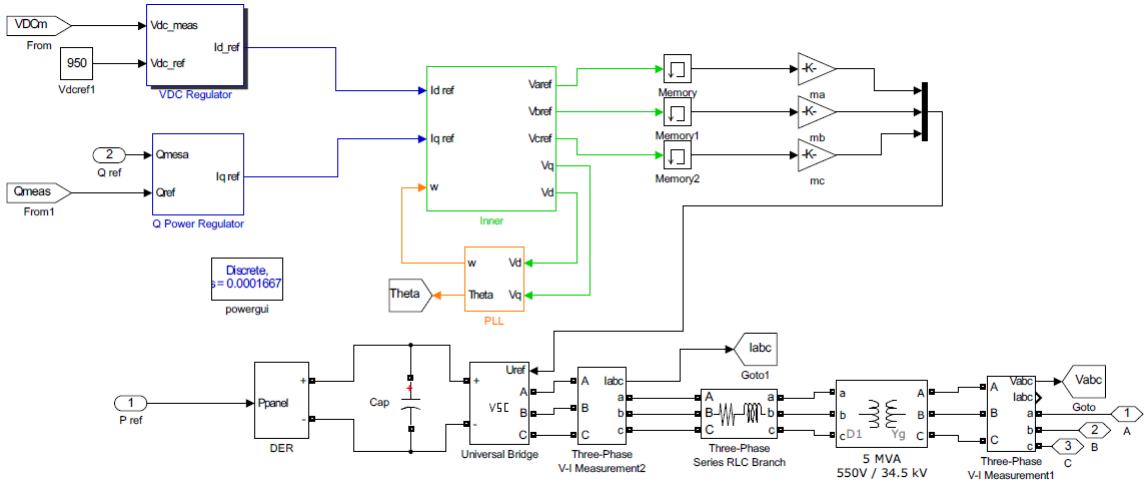

Figure 2.12: Implemented VOC control for VSC grid connected

In Figure 2.13 is shown the first order transfer functions that modelling with less complexity the injected active and reactive power by a VSC equipped with VOC strategy. In this implementation the time constants in Eqs. (2.48) and (2.49) are equals to $\tau_P = 0.041$ and $\tau_Q = 0.035$.

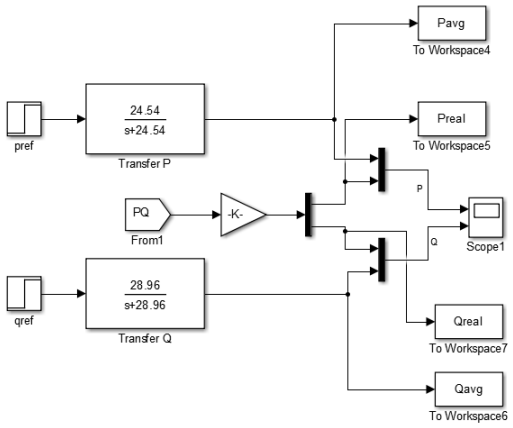

Figure 2.13: Implemented reduced model of VSC

The comparison these two models was made considering a step change in the active and reactive power. Simulations were performed in Matlab with results shown in Figure 2.14. In general, is possible appreciate that both models are similar in terms of the dynamics of the active and reactive power. Is important to notice that the dynamical responses has the characteristic of a first order model still during the transitory response, as was expected (see Figure 2.14). In the case of the complete model the dynamical response is higly related with the tuning process of the VOC PI controllers. However, the average model took only 1 second in complete the simulation with a time step of 5×10^{-5} seconds whereas the complete model required 73 seconds with a time step of 5×10^{-5}. This is only in one converter (recall that the purpose of is thesis is to study a microgrid with multiple converters).

2.6 Summary of the Chapter

In this chapter the three-phase power electronic converter model is presented. Some control modes for VSC are mentioned, to identify the most appropriate philosophy to operate the converters on islanded microgrid operation. This allow select the grid supporting mode as the indicate, since in this mode the converter have possibility of impose the frequency and voltage on the microgrid, as well as, manage the inject active and reactive power.

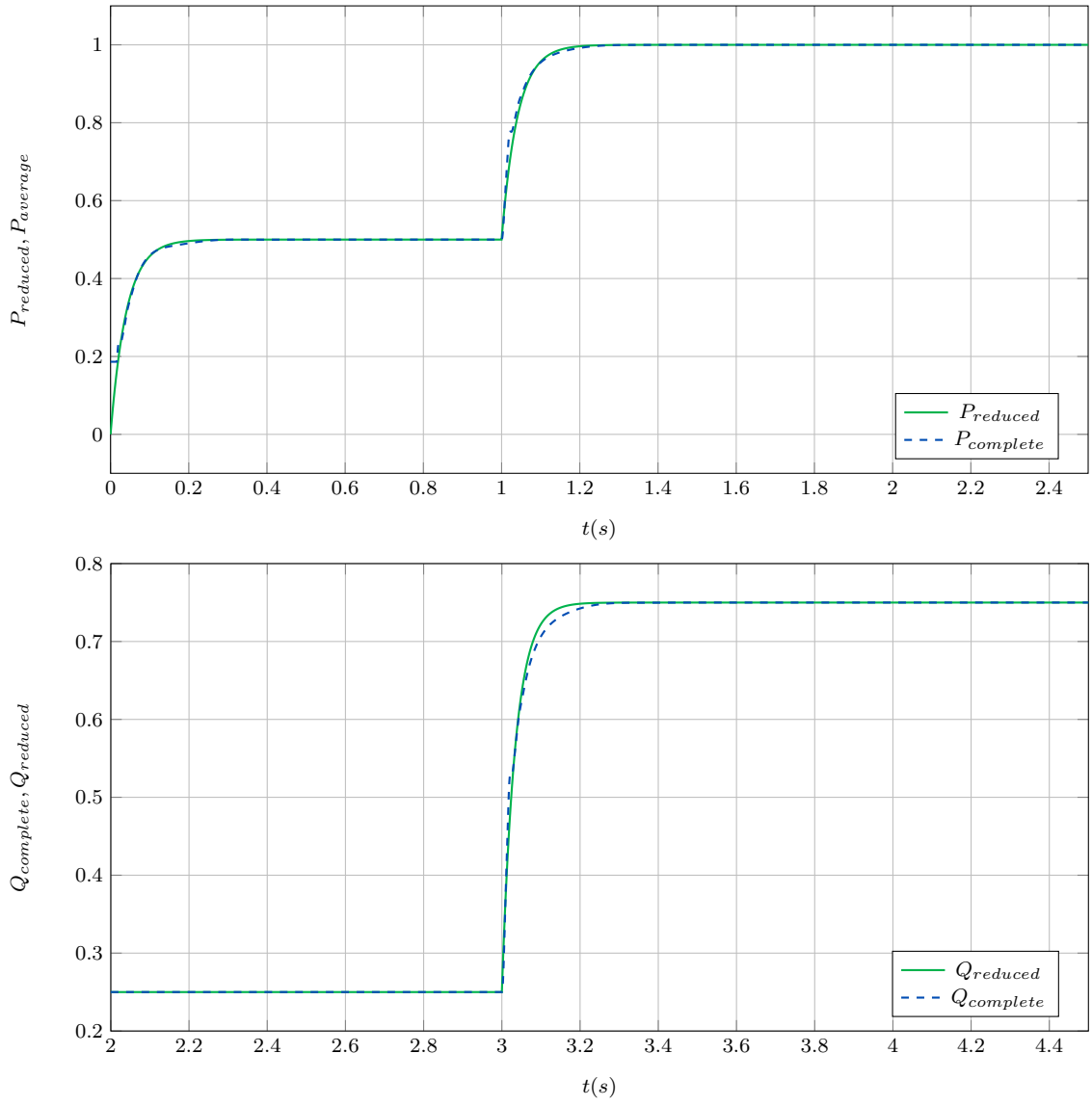

Figure 2.14: Dynamical response comparison of active and reactive power between the reduced model and the complete model of the converter, the response shows clearly the dynamical behaviour of a first order model.

The conventional vector oriented control is presented in detail, there is presented all the blocks that are responsible of control the frequency, voltage in the connection point, and the deliver power injected by the converter. A analysis of the primary control for power electronic converters is exposed, there the pure inductive and pure resistive microgrid study cases and some particularities are identified.

Also, a reduced converter model is proposed on $dq0$ reference frame, it model comprises two first order transfer functions that reproduces accurately the non-linear dynamics of the converter, it requires a reduced number of parameters to adequately represent the non-linear dynamics of the converter as is presented in Figure 2.14. However it is general enough for practical applications considering commercial converters.

Chapter 3

Model of the grid

Modern power distribution grids include massive penetration of distributed resources such as renewable energies, electric vehicles and storage devices [37]. These new technologies are integrated through three-phase power electronic converters operated under a master slave strategy in which the main grid maintain the frequency and the voltage of the grid and the converters adapt to these conditions [1]. Dynamic analysis of this type of grids require a simple enough model to be implemented computationally with the available data, but including the main physical effects of the system [38, 39].

Most of the available models for dynamic analysis of three-phase microgrids are based on a detailed model of the power-electronic converts oversimplifying the dynamics of the grid and the mutual effects among components. Although this approach is suitable for laboratory conditions where the converters are connected to a unique bus-bar and the parameters associated to the control are well known, it is not best option for real microgrids and power distribution grids where each converter is placed in different nodes and the parameters of the control are usually unknown.

Another approach consists in using a phasorial model for the grid and a detailed model of the converters [40]. This type of model is more suitable for practical applications since it includes the effect of the grid as well as the converters. However, a phasor model is an approximation of the real dynamics of the grid and the following question arises: How good is the phasor approximation in microgrid applications taking into account that the capacitance and inductance of the grid have inherent dynamics?. This chapter addresses this question by generating a model of the grid which consider the complete dynamics of the distribution lines taking into account the mutual effect among the phases.

3.1 Three-phase modeling

In stability studies of power systems know the model is a relevant factor. Thus, in this thesis a the CIGRE microgrid benchmark test system [41] is selected to make the modelling process. The original system presented in Figure 3.1, comprises a set of loads and DG grid connected initially. The amount an location of demand and generated power is not relevant in this section, such as the chapter approach is only the grid modelling.

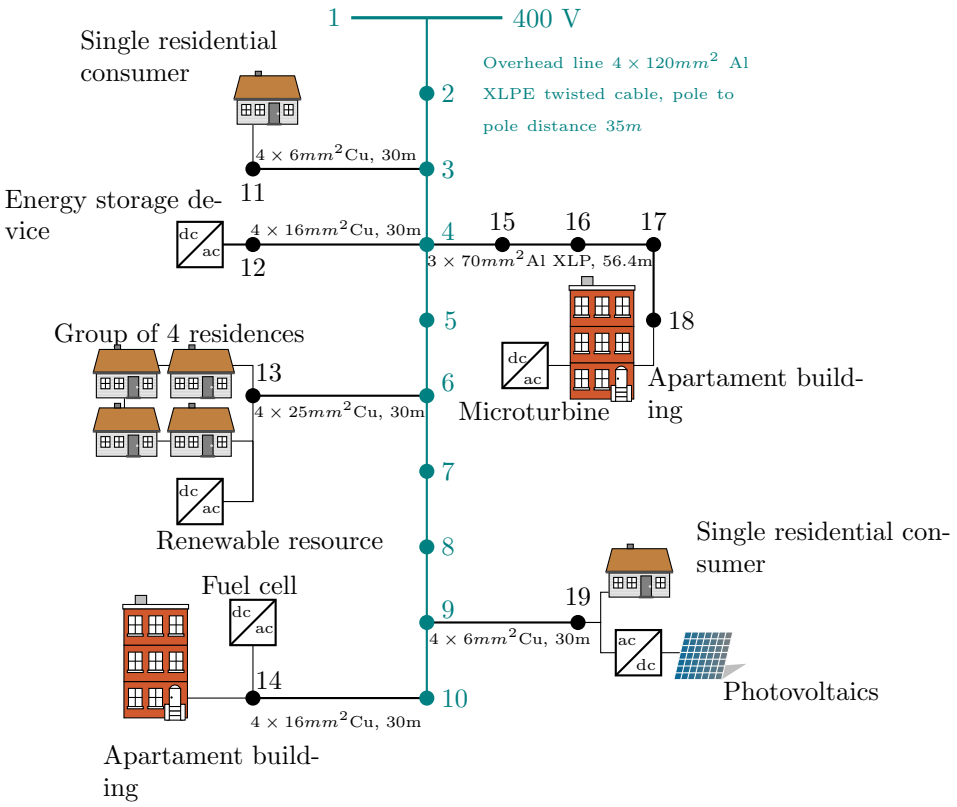

Figure 3.1: The CIGRE microgrid benchmark test system

The microgrid considers a slack node $\mathcal{S}$ and $\mathcal{N} = \{2, \ldots, k, \ldots, n\}$ nodes with power electronic converters that maintains constant active and reactive power (i.e grid following converters). Step nodes are included in the model by setting their power in zero. The set $\mathcal{E} \subseteq \mathcal{N} \times \mathcal{N}$ represents the line segment which is described by a PI-model as depicted in Figure 3.2. Each matrix in this model considers the mutual coupling between phases, thus,

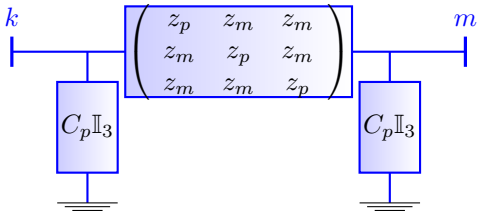

Figure 3.2: Schematic representation of a three-phase line segment in a microgrid. In this case, both the series and the shunt components are 3×3 matrices

the inductance matrix has structure presented in (3.1).

$$L = \begin{pmatrix} l_p & l_m & l_m \\ l_m & l_p & l_m \\ l_m & l_m & l_p \end{pmatrix} \tag{3.1}$$

This matrix is constructed by placing first the variables associated to the phase A, then the phase B and finally the phase C, thus, a simplified representation is obtained as given in (3.2)

$$L = \mathbb{I}_3 \otimes L_p + \mathbb{T}_3 \otimes L_m \tag{3.2}$$

where $\otimes$ is the Kronecker product, $\mathbb{I}_3$ a 3×3 identity matrix and $\mathbb{T}_3$ is a hollow matrix defined as (3.3).

$$\mathbb{T}_3 = \begin{pmatrix} 0 & 1 & 1 \\ 1 & 0 & 1 \\ 1 & 1 & 0 \end{pmatrix} \tag{3.3}$$

Additional matrices in the model have the same structure. The following matrices are defined:

$$R = \mathbb{I}_3 \otimes R_p + \mathbb{T}_3 \otimes R_m \tag{3.4}$$
$$C = \mathbb{I}_3 \otimes C_p + \mathbb{T}_3 \otimes C_m \tag{3.5}$$
$$G = \mathbb{I}_3 \otimes G_p + \mathbb{T}_3 \otimes G_m \tag{3.6}$$

The terms with subscripts p and m are 3×3 diagonal matrices, that represents the self and mutual parameters of inductances L, resistances R, capacitances C and conductances G of the system.

The incidence matrix A is calculated for the three-phase case by using $\mathbb{I}_3 \otimes A$ (see [42] for more details about the three-phase incidence matrix). For the sake of simplicity, the matrix A is separated in two sub-matrices where $A_{\mathcal{N}}$ corresponds to the nodes $\mathcal{N}$ and $A_{\mathcal{S}}$ corresponds to the slack. It is important to notice that $dim(\mathcal{S} = 3)$ meaning there are three slack nodes that correspond to each phase of the system.

The nodal voltages and branch currents are given by (3.7) and (3.8).

$$I_{\mathcal{N}} = (\mathbb{I}_3 \otimes A_{\mathcal{N}})I_{\mathcal{E}} \tag{3.7}$$

$$V_{\mathcal{E}} = (\mathbb{I}_3 \otimes A_{\mathcal{N}}^{\top})V_{\mathcal{N}} + (\mathbb{I}_3 \otimes A_{\mathcal{S}}^{\top})V_{\mathcal{S}} \tag{3.8}$$

In addition, the dynamics of line segments is given by (3.9) and (3.10).

$$V_{\mathcal{E}} = L\frac{dI_{\mathcal{E}}}{dt} + RI_{\mathcal{E}} \tag{3.9}$$

$$J_{\mathcal{N}} = C\frac{dV_{\mathcal{N}}}{dt} + GV_{\mathcal{N}} + I_{\mathcal{N}} \tag{3.10}$$

where $J_{\mathcal{N}}$ is the current injected by the converters. This current is zero at the nodes where a converter is not connected. Using the previously defined variables, the dynamical model of the microgrid is obtained, where (3.11) and (3.12) represent the dynamic behaviour of nodal voltages and branch currents as a function of the primitive parameters of elements in the system. Therefore, the model of the grid is presented as follows:

Model 1 *Dynamics of the microgrid in the reference frame abc*

$$C\frac{dV_{\mathcal{N}}}{dt} = -GV_{\mathcal{N}} + J_{\mathcal{N}} - (\mathbb{I}_3 \otimes A_{\mathcal{N}})I_{\mathcal{E}} \tag{3.11}$$

$$L\frac{I_{\mathcal{E}}}{dt} = -RI_{\mathcal{E}} + (\mathbb{I}_3 \otimes A_{\mathcal{N}}^{\top})V_{\mathcal{N}} + (\mathbb{I}_3 \otimes A_{\mathcal{S}}^{\top})V_{\mathcal{S}} \tag{3.12}$$

Considering that the slack node maintains a constant voltage with constant frequency and balanced operation, (3.13) is obtained.

$$V_{\mathcal{S}} = \begin{pmatrix} v_s \cos(\omega t) \\ v_s \cos(\omega t - 2\pi/3) \\ v_s \cos(\omega t + 2\pi/3) \end{pmatrix} \tag{3.13}$$

In addition, $J_{\mathcal{N}}$ contains constant power terminals that are integrated through a power electronic converters and therefore it presents a non-linear behaviour that was studied in Section 2.4. Notice that Model 1 is non-linear due since $J_{\mathcal{N}}$ depends on the instantaneous power as demonstrated in Chapter 2. The model is also non-autonomous due to $V_{\mathcal{S}}$ which depends on the time.

3.2 $dq0$ model representation

In order to simplify the analysis, the park transformation respect to the angle in the slack node is defined as (3.14).

$$V_{\mathcal{S}}^{dq0} = \mathbb{M} V_{\mathcal{S}}^{abc} \tag{3.14}$$

where $\mathbb{M}$ is the power invariant transformation, that is given by (3.15).

$$\mathbb{M} = \sqrt{\frac{2}{3}} \begin{pmatrix} 1/\sqrt{2} & 1/\sqrt{2} & 1/\sqrt{2} \\ \cos(\theta) & \cos(\theta - 2\pi/3) & \cos(\theta + 2\pi/3) \\ \sin(\theta) & \sin(\theta - 2\pi/3) & \sin(\theta + 2\pi/3) \end{pmatrix} \tag{3.15}$$

This transformation is applied to each voltage and current as presented in (3.16) and (3.17).

$$V_{\mathcal{N}}^{abc} = (\mathbb{M}^{-1} \otimes \mathbb{I}_n) V_{\mathcal{N}}^{dq0} \tag{3.16}$$

$$I_{\mathcal{E}}^{abc} = (\mathbb{M}^{-1} \otimes \mathbb{I}_e) I_{\mathcal{E}}^{dq0} \tag{3.17}$$

where $\mathbb{I}_n, \mathbb{I}_e$ are identity matrices. The superscripts represent the reference frame.

In order to apply these transformations to Model 1, the derivative of the transformation is obtained as (3.18).

$$\begin{aligned} \frac{d}{dt}\left((\mathbb{M}^{-1} \otimes \mathbb{I}_n) V_{\mathcal{N}}^{dq0}\right) = &\left(\frac{d\mathbb{M}^{-1}}{dt}\right) \otimes \mathbb{I}_n V_{\mathcal{N}}^{dq0} \\ &+ \left(\mathbb{M}^{-1} \otimes \mathbb{I}_n\right) \frac{dV_{\mathcal{N}}^{dq0}}{dt} \end{aligned} \tag{3.18}$$

Premultiplying (3.18) by $(\mathbb{M} \otimes \mathbb{I}_n)$ and using the properties of the Kronecker product presented in Appendix B.1 , (3.19) is obtained.

$$(\mathbb{M}\otimes\mathbb{I}_n)\frac{d}{dt}\left((\mathbb{M}^{-1}\otimes\mathbb{I}_n)V_{\mathcal{N}}^{dq0}\right)= \left(\mathbb{M}\frac{d\mathbb{M}^{-1}}{dt}\right)\otimes\mathbb{I}_nV_{\mathcal{N}}+\frac{dV_{\mathcal{N}}^{dq0}}{dt} \tag{3.19}$$

A new matrix $\mathbb{B}$ is defined as (3.20).

$$\mathbb{B}=\mathbb{M}\frac{d\mathbb{M}^{-1}}{dt}=\omega\begin{pmatrix}0&0&0\\0&0&1\\0&-1&0\end{pmatrix} \tag{3.20}$$

Notice that Matrix (3.20) is skew-symmetric. After some calculations, the following dynamical model is obtained:

Model 2 *Dynamics of the microgrid in the reference frame* $dq0$

$$\mathbb{C}\frac{dV_{\mathcal{N}}}{dt}=-\mathbb{G}V_{\mathcal{N}}-\mathbb{C}\cdot(\mathbb{B}\otimes\mathbb{I}_n)V_{\mathcal{N}}+J_{\mathcal{N}}-(\mathbb{I}_3\otimes A_{\mathcal{N}})I_{\mathcal{E}} \tag{3.21}$$

$$\mathbb{L}\frac{dI_{\mathcal{E}}}{dt}=-\mathbb{R}I_{\mathcal{E}}-\mathbb{L}\cdot(\mathbb{B}\otimes\mathbb{I}_e)I_{\mathcal{E}}+(\mathbb{I}_3\otimes A_{\mathcal{N}}^{\top})V_{\mathcal{N}}+(\mathbb{I}_3\otimes A_{\mathcal{S}}^{\top})V_{\mathcal{S}} \tag{3.22}$$

for the sake of a simplified notation, the superscript is omitted, however all variables are now in the reference frame $dq0$.

3.3 Proposed Model

The proposed microgrid model comprises a compact representation of Model 2. The structure starts by defining $x=(V_{\mathcal{N}},I_{\mathcal{E}})$ as state variables and y represents internal state variables related to each converter dynamics. So the Model 3 take the next structure.

Model 3 *Dynamics of the microgrid in the reference frame* $dq0$*: compact representation*

$$\Phi\dot{x}=-\Omega x+\Gamma x+F(x,y) \tag{3.23}$$

$$\dot{y}=g(x,y) \tag{3.24}$$

where

$$\Phi = \begin{pmatrix} \mathbb{C} & 0 \\ 0 & \mathbb{L} \end{pmatrix} \tag{3.25}$$

$$\Omega = \begin{pmatrix} \mathbb{G} + \mathbb{C} \cdot (\mathbb{B} \otimes \mathbb{I}_n) & 0 \\ 0 & \mathbb{R} + \mathbb{L} \cdot (\mathbb{B} \otimes \mathbb{I}_e) \end{pmatrix} \tag{3.26}$$

$$\Gamma = \begin{pmatrix} 0 & -A_{\mathcal{N}} \\ A_{\mathcal{N}}^{\top} & 0 \end{pmatrix} \tag{3.27}$$

$$F(x, y) = \begin{pmatrix} J_{\mathcal{N}}(x, y) \\ A_{\mathcal{S}}^{\top} V_{\mathcal{S}} \end{pmatrix} \tag{3.28}$$

Notice that Φ and Ω are posititive definite and Γ is skew-symmetric. Notice also, that the only non-linear term is $F(x, y)$ which defines the dynamics of the active components, i.e the slack node and the converters.

Now the new system parameter matrices are defined from (3.29) to (3.32).

$$\mathbb{L} = (\mathbb{M} \otimes \mathbb{I}_e) L (\mathbb{M}^{-1} \otimes \mathbb{I}_e) \tag{3.29}$$
$$\mathbb{R} = (\mathbb{M} \otimes \mathbb{I}_e) R (\mathbb{M}^{-1} \otimes \mathbb{I}_e) \tag{3.30}$$
$$\mathbb{C} = (\mathbb{M} \otimes \mathbb{I}_n) C (\mathbb{M}^{-1} \otimes \mathbb{I}_n) \tag{3.31}$$
$$\mathbb{G} = (\mathbb{M} \otimes \mathbb{I}_n) G (\mathbb{M}^{-1} \otimes \mathbb{I}_n) \tag{3.32}$$

Notice that these matrices are constant, taking into account Equations (3.2) to (3.6). In fact, these equations are simplified by using properties of the Kronecker product as follows:

$$\mathbb{L} = \mathbb{I}_3 \otimes L_p + \mathbb{K}_3 \otimes L_m \tag{3.33}$$
$$\mathbb{R} = \mathbb{I}_3 \otimes R_p + \mathbb{K}_3 \otimes R_m \tag{3.34}$$
$$\mathbb{C} = \mathbb{I}_3 \otimes C_p + \mathbb{K}_3 \otimes C_m \tag{3.35}$$
$$\mathbb{G} = \mathbb{I}_3 \otimes G_p + \mathbb{K}_3 \otimes G_m \tag{3.36}$$

where

$$\mathbb{K}_3 = \mathbb{M}\mathbb{T}_3\mathbb{M}^{-1} = diag(2, -1, -1) \tag{3.37}$$

notice this matrix is constant despite being dependent on $\mathbb{M}$.

3.4 Average model

For a more suitable analysis and results visualization, in this section an average microgrid model is proposed. This model is based on the incremental Model 4 that results of make a change of variables and find a equilibrium point of the system, as is presented in (3.38) and (3.39).

Model 4 *Given an equilibrium point $\tilde{x}$ to Model 3 and defining $\Delta x = x - \tilde{x}$ the incremental model is proposed.*

$$\Phi \Delta \dot{x} = -\Omega \Delta x + \Gamma \Delta x + F(x, y) - F(\tilde{x}, \tilde{y}) \tag{3.38}$$

$$\tau \Delta \dot{y} = \Delta S - \Delta y \tag{3.39}$$

In this case, $\Delta S = (\Delta P, \Delta Q)$. Notice that Model 4 is completely equivalent to Model 3. The time response of the system is strongly influenced by matrices Φ and τ in Model 4. However, in general $\|\Phi\| << \|\tau\|$ [43]. Therefore, the set of equations (3.38) and (3.39) can be simplified as the differential-algebraic set of equations presented in (3.40) and (3.41)

Model 5 *Average model*

$$0 = -\Omega \Delta x + \Gamma \Delta x + F(x, y) - F(\tilde{x}, \tilde{y}) \tag{3.40}$$

$$\tau \Delta \dot{y} = \Delta S - \Delta y \tag{3.41}$$

Notice that (3.40) is in fact an algebraic loop which can generate convergence problems in solvers such as Simulink. However, it can be easily managed by a direct computation of the Euler method taking into account that (3.41) does not depend on x. The values of x are obtained by solving the algebraic system (3.40) in each iteration using the method that will be presented in Section 4.1.

The suitability of this model is related with the time constants of the entire system. A microgrid that incorporate power electronic converters is a system-of-systems and the model reduction can be done in two ways. The first possibility is to build a model of the entire system and reduce it collectively, whereas the second is to reduce each converter model individually before linking them into a system. The first is more accurate since it retains all the details of the interconnected system before reduction. On the other hand,the second has the advantage of better scalability and lower computational complexity [44]. In the specific study case the advantages of this two routes are integrated in order to proposed a efficient method to reduce the microgrid model in real applications as is presented in the results section. Since a simplified model of the converter is proposed and then the model of the complete system is reduced.

3.5 Results

In this section a set of simulations are performed in order to demonstrate the accuracy and the advantages of the proposed modelling methodology. First, the equilibrium point of the entire microgrid is obtained using Model 3. This model is compared to the conventional three-phase power flow. After that, the dynamics of the microgrid is analyzed using Model 4 and Model 5. All simulations are developed in Matlab considering the parameters of the CIGRE microgrid benchmark test system shown in Figure 3.1.

Model 3 is evaluated using the Euler method coded in Matlab. It requires 0.8382 seconds to run with the loads given by the CIGRE microgrid benchmark test system [41]. The load flow results in abc reference frame are also calculated and compared to the Model 3 results in the $dq0$ reference frame. This allow conclude that the modelling method has high accuracy as is presented in Table. 3.1.

Evaluation of the averaging model is proposed to validate the averaging method, that consist in approximate the original system (3.23) and (3.24) by the averaged system (3.40) and (3.41), which is easier to study and allow infer dynamics properties of the original system. This both models are implemented in a script of Matlab and the dynamical behavior is check using the fixed point proposed method that will be exposed in the next chapter. The results are presented in Figure 3.3. It clearly shown that the models response are very similar even during the transient, validating that is possible to transform a non-linear differential equation system in a algebraic system to analysis studies, validating the averaging theory.

3.6 Summary of the Chapter

In this chapter was presented a methodology to modelling three-phase power systems. The modelling process started with a complete three-phase transmission lines representation (considering the couplings between phases), using the Kronecker product theory (Model 1). This model was complemented with the proposed simplified converter model already presented in Chapter 2. After that, a $dq0$ model representation (Model 2) was presented, using some Kronecker product properties and some demonstrable considerations about of the Park's transformation. This model allows to analyze the dynamic properties more easier than in the sinusoidal regimen.

From the $dq0$ microgrid model a compact representation (Model 3) was also presented,

Node	Voltages axis 0 [pu]		Voltages axis d [pu]		Voltages axis q [pu]	
N	Proposed Method	Load Flow	Proposed Method	Load Flow	Proposed Method	Load Flow
1	0	0	1.00	1.00	0	0
2	0	0	0.98	0.98	0.08	0.08
3	0	0	0.97	0.97	0.16	0.16
4	0	0	0.95	0.95	0.22	0.22
5	0	0	0.95	0.95	0.26	0.26
6	0	0	0.95	0.95	0.30	0.30
7	0	0	0.94	0.94	0.32	0.32
8	0	0	0.94	0.94	0.35	0.35
9	0	0	0.94	0.94	0.36	0.36
10	0	0	0.94	0.94	0.37	0.37
11	0	0	0.99	0.99	0.19	0.19
12	0	0	0.91	0.91	0.22	0.22
13	0	0	0.96	0.96	0.30	0.30
14	0	0	0.95	0.95	0.37	0.37
15	0	0	0.95	0.95	0.24	0.24
16	0	0	0.95	0.95	0.25	0.25
17	0	0	0.96	0.96	0.26	0.26
18	0	0	0.97	0.97	0.26	0.26
19	0	0	0.96	0.96	0.40	0.40

Table 3.1: Results of voltages in $dq0$ reference frame with power flow and proposed method.

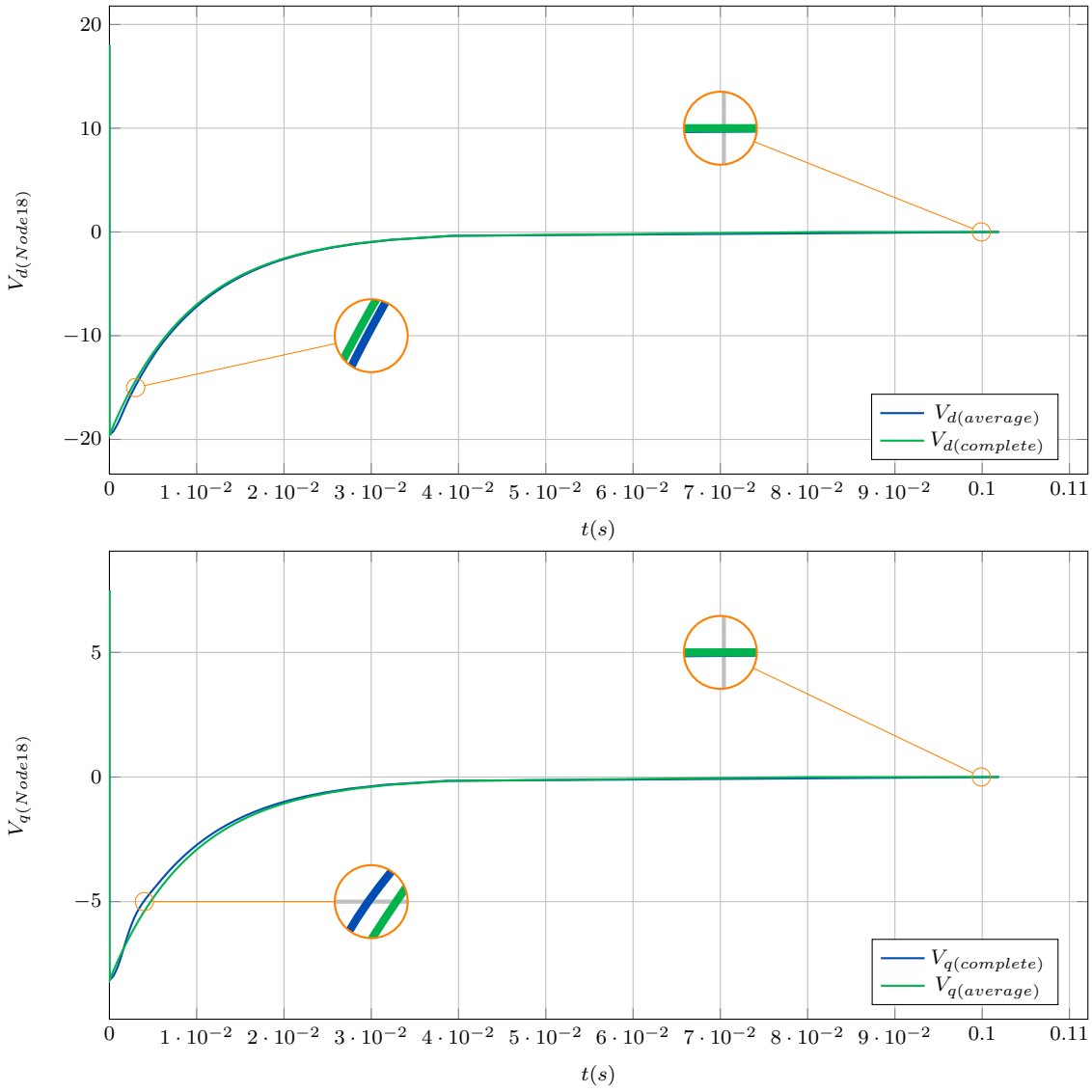

Figure 3.3: Dynamical behavior comparison of voltages from the complete and average models in d and q reference frame on node 18

this model has a state space structure, where the state variables are the nodal voltages and line currents and the outputs are the power injected by the converters. Next, an asymptotic grid model (Model 4) and an average grid (Model 5) were proposed using the averaging theory. Finally some simulations validating the accuracy of the proposed models.

Chapter 4

Equilibrium point

The next step after having the power system model comprises to find the system equilibrium point. In electric power systems it is traduced to solve the power flow problem. The power flow is a classic problem that has been widely addressed in power systems and power distribution applications. However, such methods require a constant update since the electrical systems are undergoing a transformation due to the new concept of microgrids [45]. This has resulted in the development of solutions to solve the problem in microgrids operating in islanded mode [46]- [47]. Backward/forward sweep load flow methods for radial microgrids has been proposed in [48] and [49], establishing the frequency of the system as an unknown variable to justify the absence of the slack node; contrary to the structure of conventional approaches these techniques require the grid to be radial, an assumption that is not always valid in all microgrids.

In [50] a power flow algorithm incorporating the frequency variations for ring topology balanced networks is proposed, based on the classical Newton's method. However, this methodology consider the Y_{BUS} as constant, despite being dependent on the frequency. Others works related to Newton's methods for solving the power flow problem are proposed, in [51], [52] and [53]. In [51] a power flow model for microgrids with droop control and virtual impedance is proposed for systems with low r/x ratio. On the other hand, [52] shows a power flow algorithm for hybrid ac-dc microgrids, where the set of non-linear equations are solved in an augmented trust region Newton Raphson method (NRM); in [53] a NRM was presented including the frequency deviation, where the Jacobian matrix is computed in the same way that the classical method adding the derivative of active and reactive power nodal droop functions using the derivative of each term of the Y_{bus}, but here the authors assign a slack node of the system as a reference, something that is not totally true in islanded opera-

tion.

Following the objective of this thesis the equilibrium point is important to make the small signal stability analysis. In this chapter a non-conventional way to find the equilibrium point is proposed, a fixed point iteration similar to the Gauss method is proposed for this task. Also, a modified Newton's method is presented as another alternative, however, as is presented in the following.

4.1 $dq0$ Contraction Mapping Model

In this section is exposed a $dq0$ power flow that allows compute the equilibrium point of any microgrid. The proposed model is based on some considerations applied on grid models proposed in the previous chapter. The objective is to identify the equilibrium point and present the incremental Model 4, adequate for the visualization and analysis of the results, as is mentioned in Chapter 3. In steady state, $\dot{x} = 0$ and $\dot{y} = 0$ in Model 3, so the values of x are the focus of interest since $y_P \to P$ and $y_Q \to Q$, as is possible identify on the simplified converter model (2.48) and (2.49) proposed in Chapter 2.

The model is based on a constant matrix H defined as is given in (4.1).

$$H = (\Omega - \Gamma)^{-1} \tag{4.1}$$

Therefore, the equilibrium point can be obtained as the fixed point given in (4.2)

$$x = H \cdot F(x) \tag{4.2}$$

Then, the equilibrium point is obtained by the fixed point iteration proposed in (4.3).

$$x^{(i+1)} = H \cdot F(x^{(i)}) \tag{4.3}$$

where i represents the iteration. The complete algorithm is presented as Algorithm 1. Where ϵ is the tolerance of the algorithm and $x_{initial}$ are the initial values of the voltages and currents. Notice that, unlike the conventional power flow analysis, both voltages and currents are calculated directly in the proposed method (recall that $x = (V_{\mathcal{N}}, I_{\mathcal{E}})$). Notice also that the matrix H is calculated only at the beginning of the algorithm and does not require to be actualized in each iteration. Also, the proposed method does not require per unit representation since the entire modelling is formulate in real values. This does not affect

Algorithm 1 Fixed point iteration

$y_P \leftarrow P$
$y_Q \leftarrow Q$
$H \leftarrow (\Omega - \Gamma)^{-1}$
$x \leftarrow x_{initial}$
$\delta \leftarrow \infty$
while $\delta \leq \epsilon$ **Procedure:**
  $x \leftarrow HF(x)$
  $\delta \leftarrow \|x - HF(x)\|$
end while
return x

the convergence as it is demonstrated on the results section.

The algorithm 1 is a technique used to compute the microgrid equilibrium point in both operation modes grid connected and islanded operation. For the case of grid conected mode is only necessary to apply the algorithm 1 to find the equilibrium point. In order to reach the thesis main objective, is necessary calculate the equilibrium point on islanded operation mode, to achieve this in the next section is exposed an methodology that allows find the equilibrium point using the grid connected model.

4.2 Islanded operation

The proposed methodology is based in a optimization problem, were, the objective function minimize the slack injected current and the restrictions are composed by the microgrid Model 4, as is presented in (4.4). At the end of the optimization process the problem gives the islanded microgrid equilibrium voltages and currents. Graphically this idea is shown in Figure 4.1, there is possible to notice in a electrical way what is the action carried out by optimization process into the electrical system.

$$\left.\begin{aligned} &\min \|I_s\| \\ \text{subject to} \quad & \\ &X = T(x, w) \end{aligned}\right\} \tag{4.4}$$

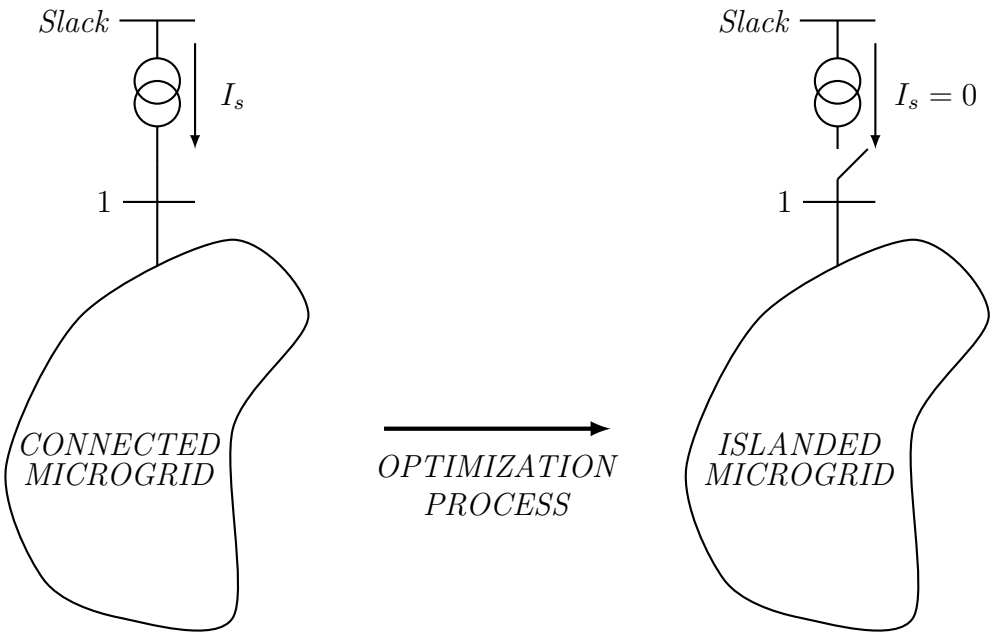

Figure 4.1: Electrical interpretation of optimization process results, to find the islanded equilibrium point

The method hypothesis is derived from the exist relationship between the current flow through the line that interconnects the microgrid with the main grid I_s, the microgrid angular frequency w and slack voltage V_s. Such relationship can be thought as a multi-variable function, i.e $I_s = f(w, V_s)$. To validate the hypothesis the used methodology varies w and V_s until to find the values that satisfies $I_s = 0$, in other words that the microgrid is operate on islanded mode. To understand the proposed concept, in Figure 4.2 is illustrate the expected evolution in the solution that will deliver the optimization process.

To validate the proposed method, in section 4.4 is presented the equilibrium point for the CIGRE microgrid using the proposed microgrid Model 4. Other option to find the equilibrium is using the mentioned Newton's method, although this method is widely used on interconnected grids in this case it does not represent a good solution since it does not consider the change on the frequency of the grid. Looking the use of it, a series of modifications to the conventional Newton's power flow that consider the islanded grid operation are proposed in the following.

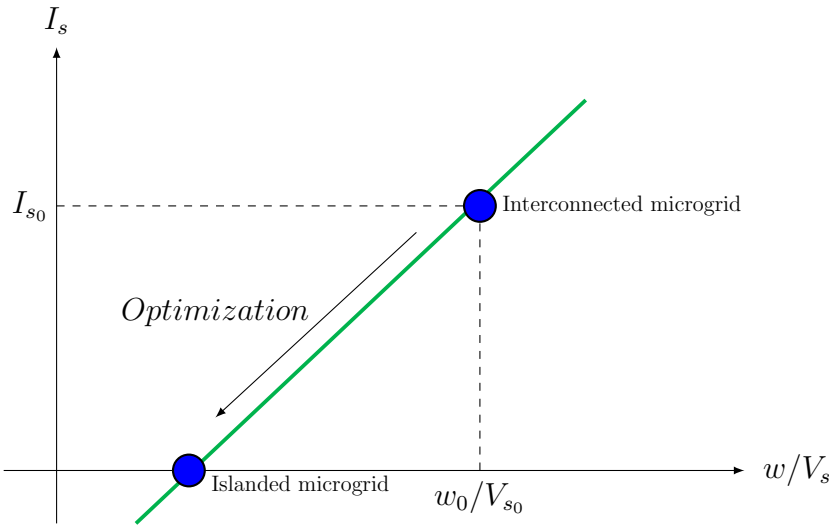

Figure 4.2: Dynamical evolution of optimization problem solution.

4.3 Phasor modelling of the grid

This section present a detailed phasorial grid modelling formulation incorporating frequency variations in ac islanded droop-controlled microgrids. The approach is general for radial and meshed grids considering an arbitrary relation r/x, also include the model of droop controls on the frequency and the voltage. Derivative of the Y_{BUS} is explicitly performed, an issue that is whether neglected or calculated numerically in conventional approaches.

To start, consider a microgrid in islanded operation represented by a connected graph $\mathcal{G} = (\mathcal{N}, \mathcal{E})$ where $\mathcal{N} = \{1, 2, \ldots, n\}$ are the nodes and $\mathcal{E} \subset \mathcal{N} \times \mathcal{N}$ are the branches. To ensure the correct analysis of this point in microgrids, three aspects must be taken into account: 1) The absence of reference or slack bus which is able to maintain bus voltage and f constants, 2) the frequency variation, 3) the change in Y_{bus} matrix according to the frequency. Considering these aspects, the power flow problem formulation start with the description of the relation between the nodal voltages $V_{\mathcal{N}}$ and branch currents $I_{\mathcal{E}}$.

From the node-branch incidence matrix $[A]$ the relation between voltages and currents

can be established as follows:

$$I_{\mathcal{N}} = [A]I_{\mathcal{E}} \tag{4.5}$$

$$V_{\mathcal{E}} = [A]^T V_{\mathcal{N}} \tag{4.6}$$

Now, the nodal currents and branch voltages can be represented in fasorial way, considering the PI transmission line model with line impedance shown in Figure 4.3, that interconnects two adjacent nodes in the microgrid.

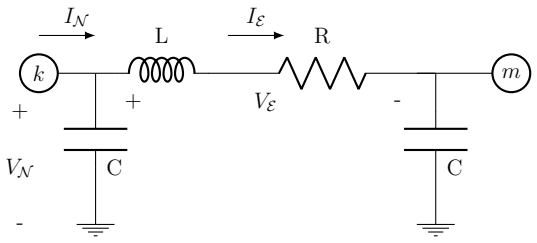

Figure 4.3: Diagram of single-phase PI transmission line

where on the line:

$$V_{\mathcal{E}} = jwLI_{\mathcal{E}} + RI_{\mathcal{E}} \tag{4.7}$$

Following in the process to find an expression for the Y_{bus} matrix, the first step is replace (4.6) in (4.7) to transform the branch voltages in a nodal variable form, so:

$$A^T V_{\mathcal{N}} = jwLI_{\mathcal{E}} + RI_{\mathcal{E}} \tag{4.8}$$

$$A^T V_{\mathcal{N}} = (jwL + R)I_{\mathcal{E}} \tag{4.9}$$

$$(jwL + R)^{-1} A^T V_{\mathcal{N}} = I_{\mathcal{E}} \tag{4.10}$$

Pre-multiplying (4.10) by $[A]$ on both sides and replace (4.5) in (4.11), results:

$$A(jwL + R)^{-1} A^T V_{\mathcal{N}} = AI_{\mathcal{E}} \tag{4.11}$$

$$A(jwL + R)^{-1} A^T V_{\mathcal{N}} = I_{\mathcal{N}} \tag{4.12}$$

Now, considering the shunt elements the Ybus matrix has the following form:

$$A(jwL + R)^{-1} A^T V_{\mathcal{N}} = I_{\mathcal{N}} - jwCV_{\mathcal{N}} \tag{4.13}$$

$$A(jwL + R)^{-1} A^T V_{\mathcal{N}} + jwCV_{\mathcal{N}} = I_{\mathcal{N}} \tag{4.14}$$

$$(A(jwL + R)^{-1} A^T + jwC)V_{\mathcal{N}} = I_{\mathcal{N}} \tag{4.15}$$

Finally, the frequency-dependent expression for the Y_{bus} has the following form:

$$Y_{Bus}(w) = A(jwL + R)^{-1}A^T + jwC \tag{4.16}$$

With this in mind, it is possible to formulate the power flow based on the Newton's method where the active (P), reactive (Q) power generations and Jacobian matrix (J) are depend of the angle and voltages on the buses and the Y_{BUS} parameters [50], as follows :

$$P_N = f_P(v, \theta, Y_{bus}) \tag{4.17}$$

$$QN = f_Q(v, \theta, Y_{bus}) \tag{4.18}$$

$$J = \begin{pmatrix} \frac{\partial f_P}{\partial \theta} & \frac{\partial f_P}{\partial v} \\ \frac{\partial f_Q}{\partial \theta} & \frac{\partial f_Q}{\partial v} \end{pmatrix} \tag{4.19}$$

On the other hand, recall that when the microgrid operate in islanded mode the power converters that incorporate the DG units should have an scheme of primary control, that generally is based in a frequency/active power (w/P) and voltage/reactive power (V/Q) droop control presented in section 2.3. Therefore, the above expressions (4.17) and (4.18) take the following form:

$$P_{ref} + K_P(w - w_0) - f_P(v, \theta, Y_{bus}(w)) = f_1 \tag{4.20}$$

$$Q_{ref} + K_Q(|V| - V_{ref}) - f_Q(v, \theta, Y_{bus}(w)) = f_2 \tag{4.21}$$

Another feature of islanded microgrids is the absence of slack bus, this brings as a consequence that system frequency is not defined, so it is clear that the set of Equations (4.20) and (4.21) gives a non-linear system of $2N$ equations with $2N + 1$ variables, thus to ensure the solution of the proposed method the system can be referred to the inertia center through the adding of the next expression:

$$\sum K_{P_i}\theta_i = 0 \tag{4.22}$$

In a vector representation, (4.22) will be:

$$K_P^T\theta = f_3 \tag{4.23}$$

Hence, the Jacobian matrix for the non-conventional frequency dependent power flow, take the next augmented form:

$$J = \begin{pmatrix} \frac{\partial f_1}{\partial \theta} & \frac{\partial f_1}{\partial v} & \frac{\partial f_1}{\partial w} \\ \frac{\partial f_2}{\partial \theta} & \frac{\partial f_2}{\partial v} & \frac{\partial f_2}{\partial w} \\ \frac{\partial f_3}{\partial \theta} & \frac{\partial f_3}{\partial v} & \frac{\partial f_3}{\partial w} \end{pmatrix} \tag{4.24}$$

The terms $J11$, $J12$ and $J21$ are computed as in the conventional Newton power flow way, while the $J13$, $J22$, $J23$, $J31$, $J32$ and $J33$ are calculated as follows:

$$J13 = \frac{\partial f_1}{\partial w} = K_P - \frac{\partial f_P}{\partial w} \tag{4.25}$$

$$J22 = \frac{\partial f_2}{\partial w} = K_Q - \frac{\partial f_Q}{\partial V} \tag{4.26}$$

$$J23 = \frac{\partial f_2}{\partial w} = -\frac{\partial f_Q}{\partial w} \tag{4.27}$$

$$J31 = \frac{\partial f_3}{\partial \theta} = K_P^T \tag{4.28}$$

$$J32 = \frac{\partial f_3}{\partial v} = 0 \tag{4.29}$$

$$J33 = \frac{\partial f_3}{\partial w} = 0 \tag{4.30}$$

4.3.1 Y_{BUS} derivative

In order to compute the term $\frac{\partial f_P}{\partial w}$ in (4.25) and $\frac{\partial f_Q}{\partial w}$ in (4.27), it is necessary derive (4.16) and use the implicit function theorem. Initially is defined:

$$Y_{Bus}(w) = AY_{Prim}A^T + jwC \tag{4.31}$$

where:

$$Y_{Prim}(w) = (jwL + R)^{-1} \tag{4.32}$$

Then the derivative of the Y_{Bus} is calculate as following:

$$\frac{\partial Y_{Bus}}{\partial w} = A\frac{\partial Y_{Prim}}{\partial w}A^T + jC \tag{4.33}$$

from (4.32)

$$(jwL + R)Y_{Prim}(w) = 1_{\mathcal{N}} \tag{4.34}$$

where $1_{\mathcal{N}}$ represents the identity matrix. Now, (4.34) is derived as follows:

$$0 = (jwL + R)\frac{\partial Y_{Prim}}{\partial w} + jLY_{Prim} \tag{4.35}$$

$$\frac{\partial Y_{Prim}}{\partial w} = -(jwL + R)^{-1} jLY_{Prim} \tag{4.36}$$

$$\frac{\partial Y_{Prim}}{\partial w} = -Y_{Prim} jLY_{Prim} \tag{4.37}$$

Finally, the $\frac{\partial f_P}{\partial w}$ and $\frac{\partial f_Q}{\partial w}$, can be obtained respectively as the real and imaginary part of resulting expression before of substitute (4.37) in (4.33):

$$\frac{\partial Y_{Bus}}{\partial w} = -AY_{Prim} jLY_{Prim} A^T + jC \tag{4.38}$$

4.3.2 Proposed Power Flow for Islanded Microgrids

The Newton's method applied to solve the flow power problem in electric power system, consider a $2N$ dimension state vector $\bar{X}$ and a set of non-linear vector equations $\bar{G}$ that can be represented as:

$$\bar{G}(\bar{X}) = 0 \tag{4.39}$$

The solution consist in found the state vector value that satisfies (4.39), this problem is solved linearising the vectorial equation using Taylor series in each iteration k, so:

$$\bar{G}(\bar{X}^k + \Delta\bar{X}^k) = \bar{G}(\bar{X}^k) + \bar{G}'(\bar{X}^k)\Delta\bar{X}^k + \bar{G}''(\bar{X}^k)\frac{\Delta\bar{X}^{k^2}}{2!} + ... + \bar{G}^n(\bar{X}^k)\frac{\Delta\bar{X}^{k^n}}{n!} \tag{4.40}$$

If in Equation (4.40) the superior order terms are neglected, 4.41 is obtain:

$$\bar{G}(\bar{X}^k + \Delta\bar{X}^k) = \bar{G}(\bar{X}^k) + J(\bar{X}^k)\Delta\bar{X}^k = 0 \tag{4.41}$$

Where, J is the Jacobian matrix (4.24) and the correction vector is obtained, as follow:

$$\bar{G}(\bar{X}^k) + J(\bar{X}^k)\Delta\bar{X}^k = 0 \tag{4.42}$$

$$-[J(\bar{X}^k)]^{-1}\bar{G}(\bar{X}^k) = \Delta\bar{X}^k \tag{4.43}$$

Adding (4.43) to the previous value of the state vector X^k the Newton's iteration procedure is formulated:

$$\bar{X}^{k+1} = \bar{X}^k - [J(\bar{X}^k)]^{-1}\bar{G}(\bar{X}^k) \tag{4.44}$$

In the proposed power flow method the $2N+1$ non-linear equations $\bar{G}(\bar{X})$ with $2N+1$ variables $\bar{X}$, is presented as a linear system $\bar{G}(\bar{X}) = [J]\Delta\bar{X}$, so:

$$\begin{bmatrix} \Delta f_1 \\ \Delta f_2 \\ \Delta f_3 \end{bmatrix} = \begin{bmatrix} J11 & J12 & J13 \\ J21 & J22 & J23 \\ J31 & J32 & J33 \end{bmatrix} \begin{bmatrix} \Delta\theta \\ \Delta V \\ \Delta w \end{bmatrix} \tag{4.45}$$

The whole procedures of the proposed power flow method for islanded microgrids are resumed in Algorithm 2.

Algorithm 2 Newton method algorithm for island microgrids

Require: Lines data (Ld)
Require: Generation and load data (GLd)
Require: Set the initial conditions (Ic) ($\mathbf{V} = 1\angle 0$ pu; $w = 1$ pu; $iter = 0$ and tolerance)
1: Calculate the incidence matrix A (Ld)
2: **Start Newton** (Ld,GLd,Ic,A,V,w)
3: **while** $Error \leq Tol$ **Procedure:**
4: iter = iter+1
5: Calculate the Y_{bus} matrix
6: Compute f_1, f_2 and f_3 Eqs. (4.20),(4.21) and (4.23)
7: Calculate Y_{bus} derivative Eq. (4.38)
8: Compute the J matrix Eq. (4.24)
9: Calculate $\Delta\theta; \Delta V; \Delta w$ Eq. (4.45)
10: Update variables From Eq. (4.44)
11: Compute Error = $Max(abs(\Delta P, \Delta Q, \Delta w))$
12: **end while**
13: **end Newton**
14: **return** V; $\delta; P_G; Q_G$ and w {These are the solution!}

4.4 Results

To validate the techniques proposed in this chapter, initially is compute the microgrid connected equilibrium point. In Figure 4.4 is presented the contraction mapping convergence graphic, there is possible observe the state variables error evolution as iteration number are

augmented, from this it is easy to notice that the method achieve high accuracy in few iterations in a quadratic way, the equilibrium point when the algorithm finishes is plot in Figure 4.5.

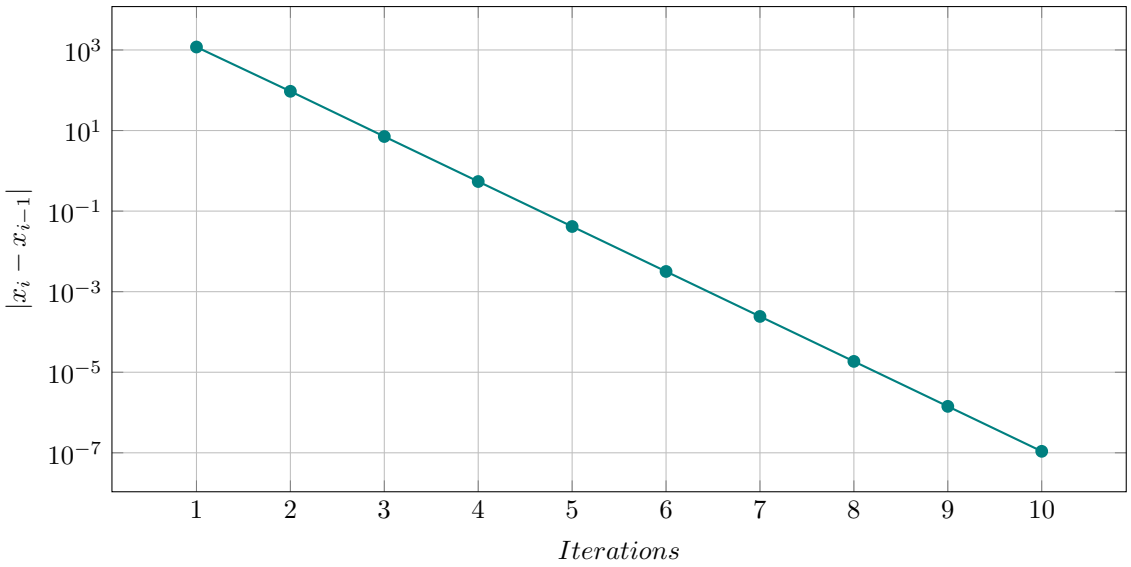

Figure 4.4: Convergence graphic of the proposed method

To analyse the dynamic behavior of the proposed model under a perturbation in the reference of active power, a change to 50% in the initial active power generate by the converters in the CIGRE microgrid benchmark test system is programmed, and the new equilibrium point is founded. The results shown that the model maintain the $dq0$ voltages on the system near the rated point. The model took into account modification in the injected currents in order to reach the programmed value on the active power as presented in Figure 4.5.

On the other hand, the islanded equilibrium point is presented in Table. 4.1 (this equilibrium take into account the initial programmed values on active and reactive power and droop constants present in the annex section). From Table. 4.1 it is worth notice that the nodal voltages are near to the expected value 1 pu even when the microgrid is operate on islanded mode, this is due to the action of droop control, the same thing pass with the grid frequency the primary control is able to stablish the value in $f = 58.89$ Hz.

In order to validate the proposed hypothesis to obtain this values in Figure 4.6 and Figure 4.7 are presented the simulation results. In Figure 4.6 is depicted the way as the grid fre-

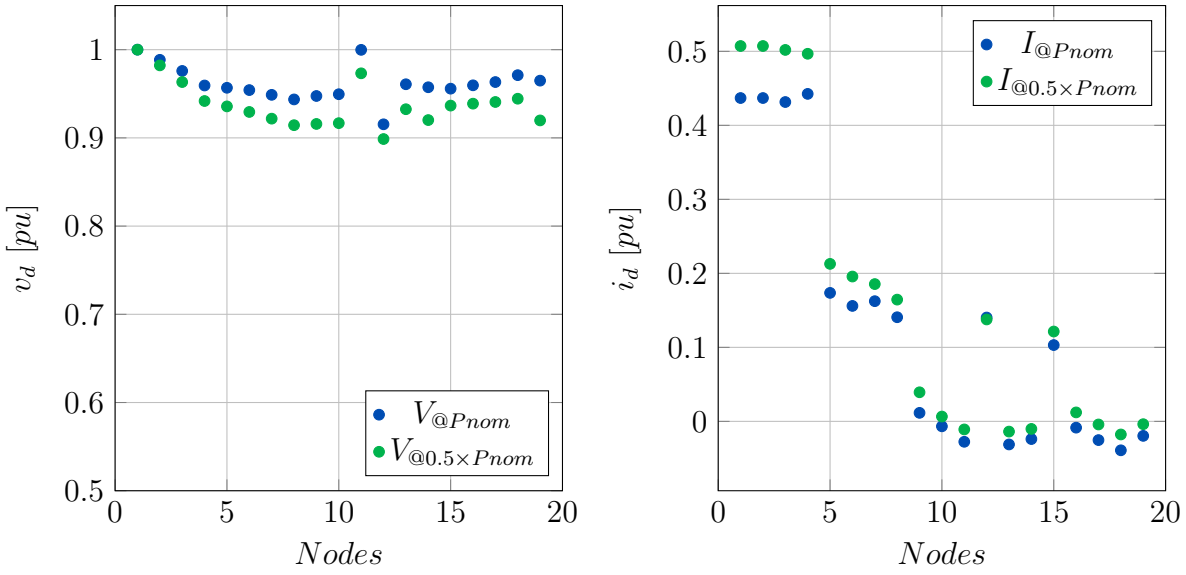

Figure 4.5: Comparison of equilibrium point when a perturbation of 50% step down in nominal active power on CIGRE microgrid was programmed.

quency and slack voltage vary, with the aim of carrying the slack current $|I_s|$ to 0 as is show in Figure 4.7. From this results is important notice that the system is now operating on islanded mode, so that the mentioned hypothesis is confirmed. Additionally in Figure 4.8 is presented graphically the solution of the optimization problem (4.4), there is shown as the slack current comes to $|I_s| = 0$ and confirm the values of w and V_s that ensure the microgrid disconnection.

A last simulation, shows as the equilibrium point computed by the proposed power flow algorithm for islanded microgrids, is similar to the calculated by the proposed optimization problem. In Table 4.2 is presented a comparison between the magnitude voltages solution from the proposed islanded Newton power flow (NIPF) and the magnitude voltages obtained with the optimization and contraction mapping method (OP-CM) presented in Table 4.1. (Recall that its voltages are in $dq0$ reference frame, so that the magnitude is determined by $|V| = \sqrt{v_0^2 + v_d^2 + v_q^2}$). The other relevant variable is the grid frequency the NIPF take 10 iterations to finish the process and this variable has a value of 59.99 Hz.

Node #	Voltages axis 0 [pu]	Voltages axis d [pu]	Voltages axis q [pu]
1	0	0.974	0
2	0	0.974	0.0001
3	0	0.973	0.0008
4	0	0.968	0.0002
5	0	0.9747	0.0044
6	0	0.9804	0.0094
7	0	0.9808	0.0131
8	0	0.9810	0.0172
9	0	0.9892	0.0243
10	0	0.9933	0.0273
11	0	1.0285	0.0118
12	0	0.9257	0.0030
13	0	0.9942	0.0120
14	0	1.0118	0.0367
15	0	0.9680	0.0018
16	0	0.9743	0.0008
17	0	0.9805	0.0006
18	0	0.9956	0.0021
19	0	1.0434	0.0641

Table 4.1: Results of islanded voltages in $dq0$ reference frame with proposed optimization method.

4.5 Summary of the Chapter

In this chapter the main objective was to find the CIGRE microgrid islanded equilibrium point, ad hoc, initially was presented a $dq0$ three-phase power flow, this is based in a contraction mapping (CM) iterative algorithm, that consider the complete microgrid model i.e lines, loads, and converters models into the system, as well as, that the microgrid is connected to the main grid. With this CM algorithm on simulations performed in Matlab was computed the equilibrium point for the grid connected microgrid, but, like this point is not the desired point, then, a homotopy that allow find the islanded equilibrium point was proposed. This idea was presented in a graphical way so that it is easily understood. The mathematical process comprises solve an optimization problem (OP) that use the CM algorithm as restrictions and the objective is minimize the slack injected current. Some simulation results was also present, such as, the islanded equilibrium point and the evolution on the OP solution.

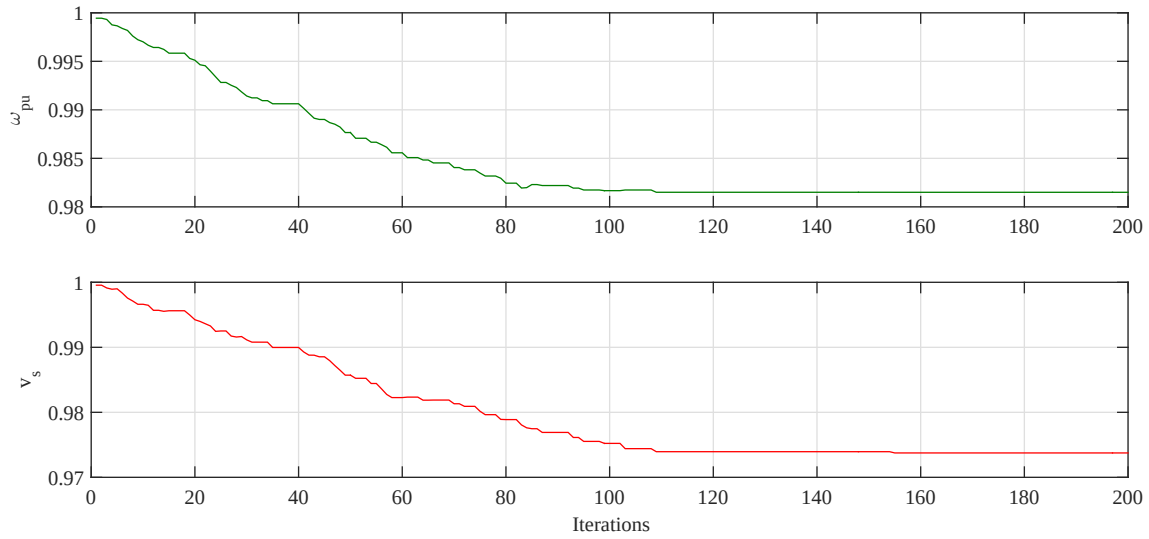

Figure 4.6: Dynamical behaviour of slack voltage and microgrid angular frequency

In order to compare and validate the results of the proposed OP-CM algorithm, a non-conventional islanded power flow based in Newton's method (NIPF) was proposed. It consider a phasor grid modelling that was also presented. The method performance was validate via simulation using the same microgrid. The results of both methods was compared and it is noticeable that there is a small difference, it is due to that the OP-CM used a more complex and detailed microgrid model, i.e coupling between phases and model converter, unlike to the NIPF that only take into account a single phase representation.

As was mentioned the proposed algorithms allow compute the microgrid equilibrium point quickly, it can gives the possibility for real time implementation. However, an inspection of the algorithms process shows that its requires the systems parameters, for example distribution lines parameters, controllers parameters of the converters, droop constants, etc. Since, these values are not always available due to the privacy in the information that is desired by the owners of the microgrid assets, some limitations may arise.

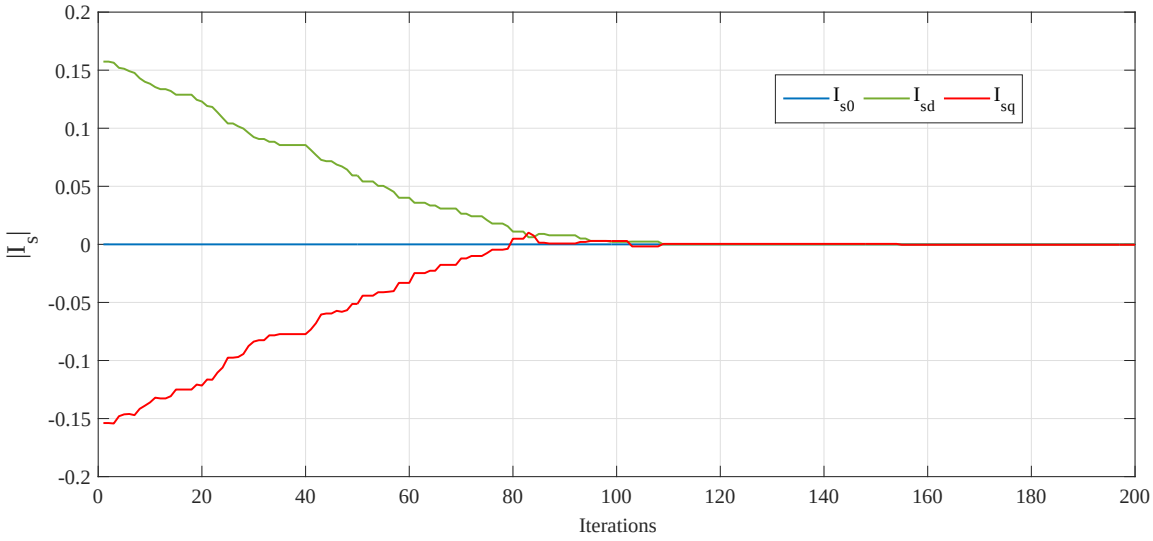

Figure 4.7: Dynamical behaviour of slack injected current.

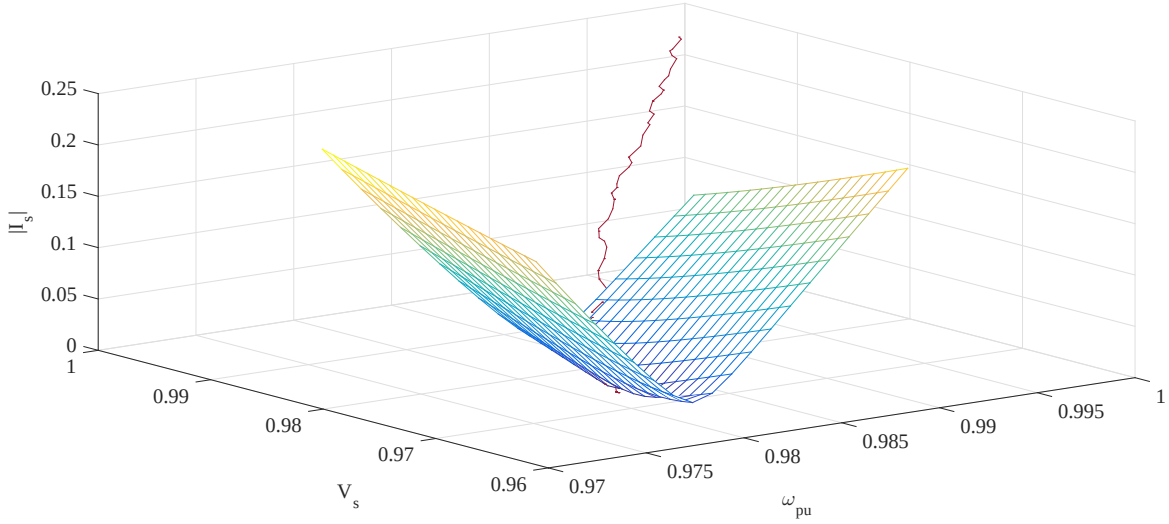

Figure 4.8: Objective function evolution and convex solution space of the proposed OP-CM method to find the islanded microgrid equilibrium point.

Node #	Voltage NIPF [pu]	Voltage OP-CM [pu]	$\|Error\|$
2	0.9870	0.9740	0.0130
3	0.9870	0.9730	0.0140
4	0.9883	0.9680	0.0203
5	0.9908	0.9747	0.0160
6	0.9932	0.9804	0.0128
7	0.9911	0.9809	0.0102
8	0.9890	0.9812	0.0078
9	0.9890	0.9895	0.0005
10	0.9924	0.9937	0.0013
11	1.0001	1.0286	0.0284
12	0.9763	0.9257	0.0506
13	0.9998	0.9943	0.0056
14	0.9999	1.0125	0.0126
15	0.9899	0.9680	0.0219
16	0.9934	0.9743	0.0191
17	0.9969	0.9805	0.0164
18	0.9999	0.9956	0.0043
19	1.0002	1.0454	0.0451

Table 4.2: Comparison of Islanded equilibrium voltages obtained with both proposed models.

Chapter 5

Small signal stability

On the scientific literature, the studies related to microgrids are mainly focus on the design of system capacity [54], system modeling and simulation [55, 56], power quality [57], power generation operation and control [58, 59], while rarely are presented stability studies [60, 61]. Thus, the study on stability of microgrids is especially important. To contextualize the stability of microgrids includes two parts:

- Transient stability (TS): It is related with large disturbances.
- Small signal stability (SSS): It is related on small disturbances sense (It is the study case of this research).

Small-signal stability (SSS) is an analysis associated with the ability of a power system to maintain synchronism in the presence of small disturbances, i.e small generation and/or load changes [18]. This analysis comprise assessing the stability of an equilibrium point. When the analysis is made under small disturbances, the system behavior can be studied via the theory of linear systems around an equilibrium point [62].

The stability of an equilibrium point can be evaluated by eigenvalue analysis according to the Lyapunov criterion [63], which states that an equilibrium is be stable in the small-signal sense, if all eigenvalues have negative real part. In the other case, the equilibrium point is unstable if at least one eigenvalue is located on the positive side of the real axis on the complex plane. This dominant eigenvalue analysis from the eigen-analysis is called the critical eigenvalue, and is possible determine the association to the state variables it is investigated through a selective modal analysis [64, 65]

In the following a linear stability analysis for the CIGRE microgrid presented in the Chapter 3 will be described, this with the aim of prove, using the eigenvalue-analysis, how is affect the stability of the system when the generation change. It is important to establish some limits of exchange power between distributed renewable resources and loads.

The dynamical microgrid model is presented in Model 2 (recall that the model is in $dq0$ reference frame), so the model has $6\mathcal{N} + 2\mathcal{C}$ differential equations with $\mathcal{N}$ equal to nodes number and $\mathcal{C}$ as the converters number into the microgrid. In model 2, V_s is the slack Voltage, and $J_{\mathcal{N}}$ is the injected current by each converter (2.46). If these model is expand in each component and the corresponding inject current is replace, the microgrid model take the following structure:

$$f_1 \rightarrow \mathbb{C}_0 \frac{dV_{\mathcal{N}_0}}{dt} = -\mathbb{G}_0 V_{\mathcal{N}_0} - \mathbb{C}_0 \cdot (\mathbb{B}_0 \otimes \mathbb{I}_n) V_{\mathcal{N}_0} - (\mathbb{I}_3 \otimes A_{\mathcal{N}}) I_{\mathcal{E}_0} \tag{5.1}$$

$$f_2 \rightarrow \mathbb{C}_d \frac{dV_{\mathcal{N}_d}}{dt} = -\mathbb{G}_d V_{\mathcal{N}_d} - \mathbb{C}_d \cdot (\mathbb{B}_d \otimes \mathbb{I}_n) V_{\mathcal{N}_d} - \frac{y_{P_{\mathcal{N}}}}{{V_{\mathcal{N}_d}}^2 + {V_{\mathcal{N}_q}}^2} V_{\mathcal{N}_d} + \frac{y_{Q_{\mathcal{N}}}}{{V_{\mathcal{N}_d}}^2 + {V_{\mathcal{N}_q}}^2} V_{\mathcal{N}_q} - (\mathbb{I}_3 \otimes A_{\mathcal{N}}) I_{\mathcal{E}_d} \tag{5.2}$$

$$f_3 \rightarrow \mathbb{C}_q \frac{dV_{\mathcal{N}_q}}{dt} = -\mathbb{G}_q V_{\mathcal{N}_q} - \mathbb{C}_q \cdot (\mathbb{B}_q \otimes \mathbb{I}_n) V_{\mathcal{N}_q} - \frac{y_{P_{\mathcal{N}}}}{{V_{\mathcal{N}_d}}^2 + {V_{\mathcal{N}_q}}^2} V_{\mathcal{N}_q} - \frac{y_{Q_{\mathcal{N}}}}{{V_{\mathcal{N}_q}}^2 + {V_{\mathcal{N}_d}}^2} V_{\mathcal{N}_d} - (\mathbb{I}_3 \otimes A_{\mathcal{N}}) I_{\mathcal{E}_q} \tag{5.3}$$

$$f_4 \rightarrow \mathbb{L}_0 \frac{dI_{\mathcal{E}_0}}{dt} = -\mathbb{R}_0 I_{\mathcal{E}_0} - \mathbb{L}_0 \cdot (\mathbb{B}_0 \otimes \mathbb{I}_e) I_{\mathcal{E}_0} + (\mathbb{I}_3 \otimes A_{\mathcal{N}}^{\top}) V_{\mathcal{N}_0} + (\mathbb{I}_3 \otimes A_{\mathcal{S}}^{\top}) V_{\mathcal{S}_0} \tag{5.4}$$

$$f_5 \rightarrow \mathbb{L}_d \frac{dI_{\mathcal{E}_d}}{dt} = -\mathbb{R}_d I_{\mathcal{E}_d} - \mathbb{L}_d \cdot (\mathbb{B}_d \otimes \mathbb{I}_e) I_{\mathcal{E}_d} + (\mathbb{I}_3 \otimes A_{\mathcal{N}}^{\top}) V_{\mathcal{N}_d} + (\mathbb{I}_3 \otimes A_{\mathcal{S}}^{\top}) V_{\mathcal{S}_d} \tag{5.5}$$

$$f_6 \rightarrow \mathbb{L}_q \frac{dI_{\mathcal{E}_q}}{dt} = -\mathbb{R}_q I_{\mathcal{E}_q} - \mathbb{L}_q \cdot (\mathbb{B}_q \otimes \mathbb{I}_e) I_{\mathcal{E}_q} + (\mathbb{I}_3 \otimes A_{\mathcal{N}}^{\top}) V_{\mathcal{N}_q} + (\mathbb{I}_3 \otimes A_{\mathcal{S}}^{\top}) V_{\mathcal{S}_q} \tag{5.6}$$

$$f_7 \rightarrow \tau_{P_{\mathcal{N}}} \frac{y_{P_{\mathcal{N}}}}{dt} = P_{\mathcal{N}} - y_{P_{\mathcal{N}}} \tag{5.7}$$

$$f_8 \rightarrow \tau_{Q_{\mathcal{N}}} \frac{y_{P_{\mathcal{N}}}}{dt} = Q_{\mathcal{N}} - y_{Q_{\mathcal{N}}} \tag{5.8}$$

The set of differentials Equations (5.1) to (5.3) has a non-linear terms, in order to applied the small signal theory this system must be linearised around at an equilibrium point, to get the state matrix and check the system eigenvalues. The process comprises write the system equations (5.1) to (5.8) in a linear state space form according to (5.9).

$$\begin{bmatrix} \Delta \dot{x}_1 \\ \Delta \dot{x}_2 \end{bmatrix} = \begin{bmatrix} A_{11} & A_{12} \\ A_{21} & A_{22} \end{bmatrix} \begin{bmatrix} \Delta x_1 \\ \Delta x_2 \end{bmatrix} + B\Delta u \tag{5.9}$$

where the state variables vector $\Delta X = [\Delta x_1, \Delta x_2]^T$ are defined as in (5.10) and Δu

represent the inputs vector. The other 4 individual sub-matrices A_{11}, A_{12}, A_{21}, A_{22} of A are composed by partial derivatives as is presented in (5.11), these 4 sub-matrices and B matrix are full detailed in annex section.

$$\Delta X = \begin{bmatrix} \Delta x_1 = \begin{bmatrix} \Delta V_{\mathcal{N}_0} \\ \Delta V_{\mathcal{N}_d} \\ \Delta V_{\mathcal{N}_q} \\ \Delta I_{\mathcal{E}_0} \\ \Delta I_{\mathcal{E}_d} \\ \Delta I_{\mathcal{E}_q} \end{bmatrix} \\ \Delta x_2 = \begin{bmatrix} \Delta y_{P_{\mathcal{N}}} \\ \Delta y_{Q_{\mathcal{N}}} \end{bmatrix} \end{bmatrix} \tag{5.10}$$

$$A = \begin{bmatrix} A_{11} = \begin{bmatrix} \frac{\partial f_1}{\partial V_{\mathcal{N}_0}} & \frac{\partial f_1}{\partial V_{\mathcal{N}_d}} & \frac{\partial f_1}{\partial V_{\mathcal{N}_q}} & \frac{\partial f_1}{\partial I_{\mathcal{E}_0}} & \frac{\partial f_1}{\partial I_{\mathcal{E}_d}} & \frac{\partial f_1}{\partial I_{\mathcal{E}_q}} \\ \frac{\partial f_2}{\partial V_{\mathcal{N}_0}} & \frac{\partial f_2}{\partial V_{\mathcal{N}_d}} & \frac{\partial f_2}{\partial V_{\mathcal{N}_q}} & \frac{\partial f_2}{\partial I_{\mathcal{E}_0}} & \frac{\partial f_2}{\partial I_{\mathcal{E}_d}} & \frac{\partial f_2}{\partial I_{\mathcal{E}_q}} \\ \frac{\partial f_3}{\partial V_{\mathcal{N}_0}} & \frac{\partial f_3}{\partial V_{\mathcal{N}_d}} & \frac{\partial f_3}{\partial V_{\mathcal{N}_q}} & \frac{\partial f_3}{\partial I_{\mathcal{E}_0}} & \frac{\partial f_3}{\partial I_{\mathcal{E}_d}} & \frac{\partial f_3}{\partial I_{\mathcal{E}_q}} \\ \frac{\partial f_4}{\partial V_{\mathcal{N}_0}} & \frac{\partial f_4}{\partial V_{\mathcal{N}_d}} & \frac{\partial f_4}{\partial V_{\mathcal{N}_q}} & \frac{\partial f_4}{\partial I_{\mathcal{E}_0}} & \frac{\partial f_4}{\partial I_{\mathcal{E}_d}} & \frac{\partial f_4}{\partial I_{\mathcal{E}_q}} \\ \frac{\partial f_5}{\partial V_{\mathcal{N}_0}} & \frac{\partial f_5}{\partial V_{\mathcal{N}_d}} & \frac{\partial f_5}{\partial V_{\mathcal{N}_q}} & \frac{\partial f_5}{\partial I_{\mathcal{E}_0}} & \frac{\partial f_5}{\partial I_{\mathcal{E}_d}} & \frac{\partial f_5}{\partial I_{\mathcal{E}_q}} \\ \frac{\partial f_6}{\partial V_{\mathcal{N}_0}} & \frac{\partial f_6}{\partial V_{\mathcal{N}_d}} & \frac{\partial f_6}{\partial V_{\mathcal{N}_q}} & \frac{\partial f_6}{\partial I_{\mathcal{E}_0}} & \frac{\partial f_6}{\partial I_{\mathcal{E}_d}} & \frac{\partial f_6}{\partial I_{\mathcal{E}_q}} \end{bmatrix} & A_{12} = \begin{bmatrix} \frac{\partial f_1}{\partial y_{P_\mathcal{N}}} & \frac{\partial f_1}{\partial y_{Q_\mathcal{N}}} \\ \frac{\partial f_2}{\partial y_{P_\mathcal{N}}} & \frac{\partial f_2}{\partial y_{Q_\mathcal{N}}} \\ \frac{\partial f_3}{\partial y_{P_\mathcal{N}}} & \frac{\partial f_3}{\partial y_{Q_\mathcal{N}}} \\ \frac{\partial f_4}{\partial y_{P_\mathcal{N}}} & \frac{\partial f_4}{\partial y_{Q_\mathcal{N}}} \\ \frac{\partial f_5}{\partial y_{P_\mathcal{N}}} & \frac{\partial f_5}{\partial y_{Q_\mathcal{N}}} \\ \frac{\partial f_6}{\partial y_{P_\mathcal{N}}} & \frac{\partial f_6}{\partial y_{Q_\mathcal{N}}} \end{bmatrix} \\ A_{21} = \begin{bmatrix} \frac{\partial f_7}{\partial V_{\mathcal{N}_0}} & \frac{\partial f_7}{\partial V_{\mathcal{N}_d}} & \frac{\partial f_7}{\partial V_{\mathcal{N}_q}} & \frac{\partial f_7}{\partial I_{\mathcal{E}_0}} & \frac{\partial f_7}{\partial I_{\mathcal{E}_d}} & \frac{\partial f_7}{\partial I_{\mathcal{E}_q}} \\ \frac{\partial f_8}{\partial V_{\mathcal{N}_0}} & \frac{\partial f_8}{\partial V_{\mathcal{N}_d}} & \frac{\partial f_8}{\partial V_{\mathcal{N}_q}} & \frac{\partial f_8}{\partial I_{\mathcal{E}_0}} & \frac{\partial f_8}{\partial I_{\mathcal{E}_d}} & \frac{\partial f_8}{\partial I_{\mathcal{E}_q}} \end{bmatrix} & A_{22} = \begin{bmatrix} \frac{\partial f_7}{\partial y_{P_\mathcal{N}}} & \frac{\partial f_7}{\partial y_{Q_\mathcal{N}}} \\ \frac{\partial f_8}{\partial y_{P_\mathcal{N}}} & \frac{\partial f_8}{\partial y_{Q_\mathcal{N}}} \end{bmatrix} \end{bmatrix} \end{bmatrix} \tag{5.11}$$

The next step to finally with the system linearisation is to evaluate each derivative term in A, on the islanded microgrid equilibrium point. So, A is a constant matrix that is depend of the conditions under the microgrid is analyzed. In what remains, the islanded microgrid stability analysis is presented using the resulting lineal state space microgrid model.

5.1 Results

Before presenting the chapter results it is important recall the main results obtained in each chapter. The Chapter 2 is dedicated to study the converter model, there the conventional model of VSC is compared whit a proposed simplified model, where a simulation result show that is possible use these simplified converter model instead of the complex complete model. With this, the model of one of relevant elements into the microgrids is defined.

The Chapter 3 is dedicated to the grid model (it comprises lines and loads), there is proposed a three-phase grid conected microgrid model i.e. there is a slack node. This three-phase model is then presented on $dq0$ reference frame and to more suitable analysis and results visualization a average model is proposed. So, with the Chapter 3 results is addressed the rest of elements into the microgrid.

The Chapter 4 collect the proposed models in the previous chapters, in order to find the equilibrium point of the CIGRE microgrid test system under a specified operative condition. To achieve it, there are proposed some algorithms that allow find that point. Other important contribution in this chapter is that both connected microgrid and islanded microgrid equilibrium points are presented.

At this point is where all the results obtained in each of the previous chapters converges. So, this section is dedicated to show the results of the eigenvalues stability analysis. Here a simply simulations will show the islanded microgrid stability under a specific operative condition.

As was mentioned above the critical eigenvalue analysis comprises compute the state matrix eigenvalues i.e. $eig(\mathrm{A})$. So, it requires initially to evaluate all the derivatives in (5.11) on the islanded equilibrium point presented in Table. 4.1. The resulting A matrix was computed in a script in Matlab, it is not presented due to the big dimensions, but instead the eigenvalues are presented in Table 5.1.

From Table 5.1 is noticeable that all the system eigenvalues has negative real part, in other words it is traduced in that the system is stable under the operative conditions presented in the section A on the annex. For studying system stability, the slow and poorly damped poles will be of main interest, and from the above listed eigenvalues it can be observed that the system has ten real poles and some complex conjugate poles close to the origin, with respect to the rest as is shown in Figure 5.1.

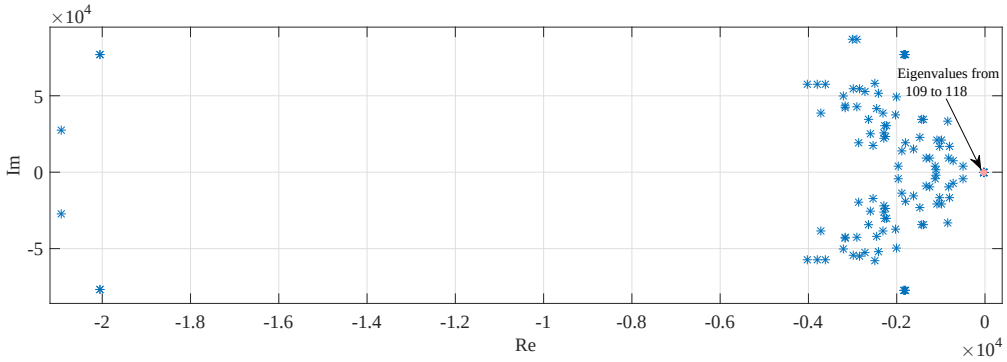

Figure 5.1: Location of microgrid system eigenvalues in complex plane

Table 5.1: Microgrid system eigenvalues under islanded operation

$\lambda_{1,2} = -2895.68 \pm j87016.53$	$\lambda_{31,32} = -2710.47 \pm j52676.55$	$\lambda_{87,88} = -1112.21 \pm j1874.17$	$\lambda_{87,88} = -2643.22 \pm j3434.05$
$\lambda_{3,4} = -2997.86 \pm j87012.30$	$\lambda_{33,34} = -2417.82 \pm j51846,95$	$\lambda_{61,62} = -2254.11 \pm j23590.84$	$\lambda_{89,90} = -2221.86 \pm j30184.95$
$\lambda_{5,6,7,8} = -20044.41 \pm j76847.71$	$\lambda_{35,36} = -3203.44 \pm j49995.90$	$\lambda_{63,64} = -1483.01 \pm j22998.63$	$\lambda_{91,92} = -2274.01 \pm j30336.54$
$\lambda_{9,10} = -1823.92 \pm j77208.05$	$\lambda_{37,38} = -2002.90 \pm j49533.44$	$\lambda_{65,66} = -1129.84 \pm j4194.37$	$\lambda_{93,94} = -1971.66 \pm j4114.50$
$\lambda_{11,12} = -1833.02 \pm j77206.08$	$\lambda_{39,40} = -2309.34 \pm j38499.50$	$\lambda_{67,68} = -727.39 \pm j7496.72$	$\lambda_{95,96} = -494.23 \pm j4072.75$
$\lambda_{13,14} = -1805.85 \pm j77120.71$	$\lambda_{41,42} = -3159.77 \pm j43327.85$	$\lambda_{69,70} = -2283.37 \pm j21964.67$	$\lambda_{97,98} = -1252.38 \pm j9438.45$
$\lambda_{15,16} = -1806.40 \pm j77120.62$	$\lambda_{43,44} = -2898.67 \pm j42673.04$	$\lambda_{71,72} = -1881.92 \pm j13721.31$	$\lambda_{99,100} = -1335.37 \pm j9198.31$
$\lambda_{17,18} = -20920.05 \pm j27536,97$	$\lambda_{45,46} = -3168.89 \pm j42369.93$	$\lambda_{73,74} = -2860.08 \pm j19529.77$	$\lambda_{101,102} = -1026.70 \pm j16738.54$
$\lambda_{19,20} = -2505.20 \pm j58084.51$	$\lambda_{47,48} = -2464.17 \pm j41855.69$	$\lambda_{75,76} = -1802,48 \pm j18987.51$	$\lambda_{103,104} = -1094.74 \pm j21001.57$
$\lambda_{21,22} = -4031.92 \pm j57524.62$	$\lambda_{49,50} = -844.46 \pm j33179.43$	$\lambda_{77,78} = -2545.34 \pm j17405.32$	$\lambda_{105,106} = -980.25 \pm j20879.23$
$\lambda_{23,24} = -3611.91 \pm j57336.68$	$\lambda_{51,52} = -1443.57 \pm j34340,14$	$\lambda_{79,80} = -1614.77 \pm j15360.88$	$\lambda_{107,108} = -793.48 \pm j16707.83$
$\lambda_{25,26} = -3804.22 \pm j57359.73$	$\lambda_{53,54} = -3715.63 \pm j38645.51$	$\lambda_{81,82} = -2022.20 \pm j37364.50$	$\lambda_{109,110,111,112,113} = -24.39$
$\lambda_{27,28} = -2993.92 \pm j54550.35$	$\lambda_{55,56} = -2295.67 \pm j25937.01$	$\lambda_{83,84} = -820.01 \pm j9361.65$	$\lambda_{114,115,116,117,118} = -28.57$
$\lambda_{29,30} = -2834.67 \pm j54719.22$	$\lambda_{57,58} = -2595.14 \pm j25384.75$	$\lambda_{85,86} = -1390.81 \pm j34279.94$	

As already seen from the eigenvalues analysis, the system is stable with the parameters and operating conditions specified in Table A.1. However, the small signal microgrid model can be utilized to investigate the dynamic characteristics of the system under various operating conditions and with various system parameters. To illustrate this, the eigenvalue trajectory of the system when sweeping the active power reference in the full operating range from -5.5 pu to 5.5 pu is shown in Figure 5.2.

As already explained, the steady state frequency and operating conditions of the system will change if the power reference is changed while the load is kept constant. However, the eigenvalues trajectory in Figure 5.2 shows that the system eigenvalues are highly influenced by the change of power reference, indicating that variations in the steady state operating due to the active power-frequency and reactive power-voltage droop will have significant impact on the microgrid stability if the changes are very large.

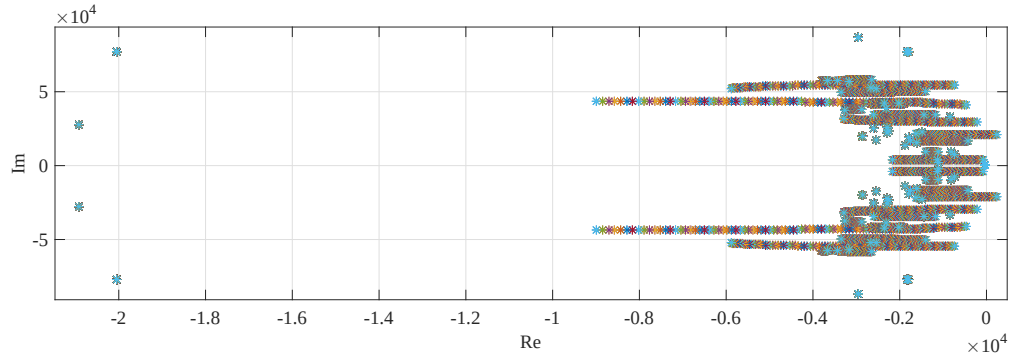

Figure 5.2: System eigenvalue trajectory with power reference swept from -5.5 pu to 5.5 pu

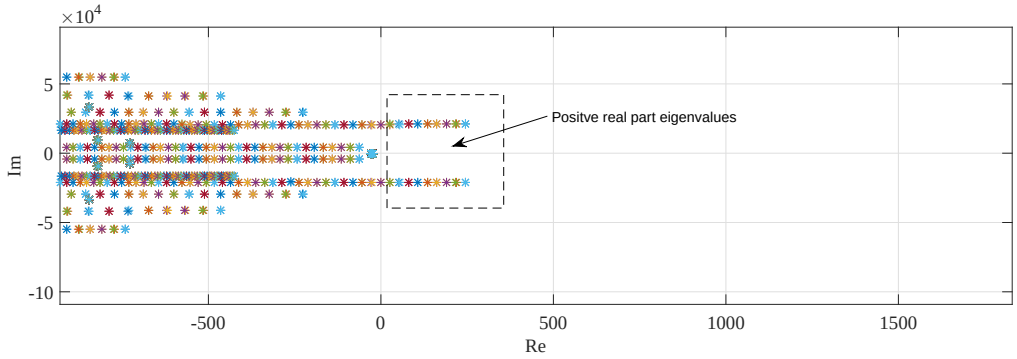

Figure 5.3: Zoom of system eigenvalue trajectory with power reference swept from -5.5 pu to 5.5 pu

5.2 Summary of the Chapter

On this chapter a small signal stability analysis for the CIGRE microgrid was described. Here a mathematical linearisation of the non-linear model for three-phase CIGRE microgrid was presented in order to analyze the system stability. The stability analysis was performed based on the eigenvalue criterion, this with the purpose of analyse the system stability under a specific operative condition.

A variety of operative cases were tested in order to compare the stability under small and big changes in the power delivered by the converters. A routine to compute the state matrix A and find the eigenvalues in each reference power value was designed. The principal test consider that the microgrid was operated in islanded mode with nominal conditions, the

stability results shows that the system is stable since all the eigenvalues are places in the complex left-half complex plane as is show in Figure 5.1.

The second section of results shows how the system eigenvalues moves as the power varies in a range that considers large and small disturbances. From here it was possible to conclude that the system is stable under small perturbations in the power delivered by the converters.

Conclusions

A complete dynamic model for three-phase microgrids and smart distribution systems was presented. The model considered the coupling effect between phases and a detailed representation of the distribution lines. A $dq0$ reference frame was selected in order to simplify the representation of the system and to obtain an autonomous dynamical system. A simplified model of the power electronic converters was also considered using the Akagui/Aredes power theory and a first order representation of the internal dynamics associated to the control. This model was compared to a complete vector oriented control. Simulation results demonstrated both models present very similar behaviour and hence, the first order model is a suitable representation for power electronic converters, with the advantage of reduced number of parameters and state variables.

The response of both the complete and the simplified models have the characteristic of a first order dynamical system. The performance demonstrated to be highly related with the tuning of the PI controllers in the VOC strategy. Thus, the dynamical response of the controllers define the order of the simplified model.

An efficient algorithm for finding the equilibrium point in the $dq0$ reference frame was also presented and tested. This algorithm was also used to generate a second model in which the dynamics associated to the inductive and capacitive components of the grid were neglected. Due to the effcient implementation of this algorithm, the model was solved and the results were similar, but with a reduced number of iterations and a larger time step. However, the complete model was prone to numerical oscillations requiring a very reduced time step. The same phenomenon was identified using Matlab-Simulink, especially when the transmission lines were modelled in detailed. Therefore, the proposed average model is an excellent alternative that can be scaled to general modelling of the power electronic converters.

The equilibrium point was also analyzed in islanded operation. In this case, the problem

was recasted as an optimization model that minimizes to zero the current that is injected by the main grid. A Newton method based on phasor representation was also proposed. These algorithms are a non-conventional way to find the equilibrium point. The equilibrium point found by both models were very similar, the small difference is related with the grid model used by each one and also with the random process used to solve the OP in the first algorithm. The model in $dq0$ considered mutual inductance between phases whereas the phaso-model was a single-phase equivalent. Since both models presented similar results, it is possible to conclude that the mutual inductance have little effect on the final results

The complete proposed $dq0$ microgrid model describes a non-linear model in time domain, therefore, a linear stability analysis was presented. This is achieved by eigenvalues analysis theory. The results showed that the primary control is capable to keep stable microgrid under small perturbations.

Future research

A random search algorithm was implemented to find the equilibrium point in islanded operation under the reference frame $dq0$. The space of feasible solutions seems to be convex, however, this was not demonstrated analytically. As future work the idea is solve this optimization problem using convex optimization in order to demonstrate convergence and global solution.

Other interesting work can be to carry out a transient stability analysis in order to evaluate some operating conditions, for example including the secondary control scheme to evaluate the change in the frecuency and voltage references in to the primary control. An equal area criteria or a method for generating Lyapunov functions is required in the stability analysis of microgrids.

Appendix A

CIGRE microgrid

The CIGRE microgrid consists of four types of elements, nodes, lines, loads and converters. This system is composed by 19 nodes including the slack node, 18 distribution lines that using 5 wire types, to supply the power delivered by converters to residential loads, as is possible to observe in Figure. 3.1.

It includes 5 non-conventional sources from all currently important (or emerging, but promising) technologies, such as photovoltaics, microturbines (CHP generation), wind turbines and fuel cells. Specific technical details, models for individual sources are beyond the scope of this thesis, so that only installation locations and sizes are indicated. The total installed capacity of the microsources and the load demand are presented in Table 7.2 and Table 7.3 respectively. The microgrid nominal power and voltage are 100 kW and 400 V.

The microgrid topology is defined in Table A.5, there are presented the lines as well as the nodes that are interconnected with its, also a coefficient that relate the line type used with the parameters of each line stretch present in Table A.6.

Table A.1: Specified locations of load and generation power values for low voltage CIGRE microgrid

Node	$P_A[kW]$	$P_B[kW]$	$P_C[kW]$	$P_{max}[kW]$	$Q_{max}[kW]$	$K_P[kW/Hz]$	$K_Q[kVAr/V]$
1	0	0	0	0	0	0	0
2	0	0	0	0	0	0	0
3	0	0	0	0	0	0	0
4	0	0	0	0	0	0	0
5	0	0	0	0	0	0	0
6	0	0	0	0	0	0	0
7	0	0	0	0	0	0	0
8	0	0	0	0	0	0	0
9	0	0	0	0	0	0	0
10	0	0	0	0	0	0	0
11	14.5	14.5	14.5	30	30	-5.50	-5.21
12	0	0	0	0	0	0	0
13	15.3	15.3	15.3	30	30	-5.60	-5.25
14	12.8	12.8	12.8	45	45	0	0
15	0	0	0	0	0	0	0
16	0	0	0	0	0	0	0
17	0	0	0	0	0	0	0
18	18.5	18.5	18.5	50	50	-5.60	-5.41
19	15.8	15.8	15.8	30	30	-5.67	-5.28

Table A.2: Converters generated power

Node	P_A [kW]	P_B [kW]	P_C [kW]
1	0	0	0
2	0	0	0
3	0	0	0
4	0	0	0
5	0	0	0
6	0	0	0
7	0	0	0
8	45	45	45
9	0	0	0
10	0	0	0
11	0	0	0
12	60	60	60
13	0	0	0
14	0	0	0
15	40	40	40
16	0	0	0
17	0	0	0
18	0	0	0
19	0	0	0

Table A.3: Load power demand

Table A.4: Microgrid topology description and wire parameters

Node 1	Node 2	Length $[m]$	Type
1	2	35	1
2	3	35	1
3	4	35	1
4	5	35	1
5	6	35	1
6	7	35	1
7	8	35	1
8	9	35	1
9	10	35	1
3	11	30	2
4	12	30	3
6	13	30	4
10	14	30	3
4	15	35	1
15	16	35	1
16	17	35	1
17	18	30	1
9	19	30	2

Table A.5: Interconnection microgrid nodes

Type	Rph $[ohm/km]$	Xph $[ohm/km]$	Ro $[ohm/km]$	Xo $[ohm/km]$	Cap $[\mu F/km]$	Name
1	0.284	0.083	1.136	0.417	0.38	OL - Twisted cable 4x120 mm2
2	3.690	0.084	13.64	0.472	0.05	SC - 4x6 mm2 Cu
3	1.380	0.082	5.520	0.418	0.18	SC - 4x16 mm2 Cu
4	0.871	0.081	3.480	0.409	0.22	SC - 4x25 mm2 Cu

Table A.6: Wires parameters

Appendix B

Mathematical Background

B.1 Properties of the Kronecker product

Given two matrices $A = [a]_{m\times n}$ and $B = [b]_{p\times q}$ then the Kronecker product $A \otimes B$ is defined as the following matrix

$$A \otimes B = \begin{pmatrix} a_{11}B & \dots & a_{1n}B \\ \vdots & & \vdots \\ a_{m1}B & \dots & a_{mn}B \end{pmatrix} \tag{B.1}$$

This product has the following properties

$$(A \otimes B)^\top = A^\top \otimes B^\top \tag{B.2}$$
$$(A \otimes B)^{-1} = A^{-1} \otimes B^{-1} \tag{B.3}$$
$$(A \otimes B)(C \otimes D) = (ac) \otimes (BD) \tag{B.4}$$
$$\partial(A \otimes B) = (\partial A) \otimes B + A \otimes (\partial B) \tag{B.5}$$
$$A \otimes (B + C) = A \otimes B + A \otimes C \tag{B.6}$$
$$A \otimes B \neq B \otimes A \ ; \ in\ general \tag{B.7}$$
$$\alpha_a A \otimes \alpha_b B = \alpha_a \alpha_b (A \otimes B) \tag{B.8}$$
$$(A \otimes h)A^{-1} = 1 \otimes h \ ; \ if\ h\ is\ a\ vector \tag{B.9}$$

B.2 State matrix A

In Chapter 5 is carry out a linearisation process, there were presented the 4-submatrices that composed the state matrix A, by space matter the full expression not were located in that section. The complete expressions to replace the equilibrium point and construct the linear system model is given in matrices (7.10) to (7.12).

$$A_{11} = \begin{bmatrix} \mathbb{C}_0^{-1}(-\mathbb{G}_0-\mathbb{C}_0\cdot(\mathbb{B}_0\otimes\mathbb{I}_n)) & 0_{18x18} & 0_{18x18} & \mathbb{C}_0^{-1}(-(\mathbb{I}_3\otimes A_{\mathcal{N}})) & 0_{18x18} & 0_{18x18} \\ 0_{18x18} & \mathbb{C}_d^{-1}(-\mathbb{G}_d-\mathbb{C}_d\cdot(\mathbb{B}_d\otimes\mathbb{I}_n))+\frac{y_P(V_{\mathcal{N}}^{d\,2}-V_{\mathcal{N}}^{q}{}^2)}{V_{\mathcal{N}}^{d\,2}+V_{\mathcal{N}}^{q\,2}} & \mathbb{C}_d^{-1}(\frac{y_Q(V_{\mathcal{N}}^{q\,2}-V_{\mathcal{N}}^{d\,2})}{V_{\mathcal{N}}^{d\,2}+V_{\mathcal{N}}^{q\,2}}) & 0_{18x18} & \mathbb{C}_d^{-1}(-(\mathbb{I}_3\otimes A_{\mathcal{N}})) & 0_{18x18} \\ 0_{18x18} & \mathbb{C}_q^{-1}(\frac{y_Q(V_{\mathcal{N}}^{d\,2}-V_{\mathcal{N}}^{d\,2})}{V_{\mathcal{N}}^{d\,2}+V_{\mathcal{N}}^{q\,2}}) & \mathbb{C}_q^{-1}(-\mathbb{G}_q-\mathbb{C}_q\cdot(\mathbb{B}_q\otimes\mathbb{I}_n))+\frac{y_P(V_{\mathcal{N}}^{q\,2}-V_{\mathcal{N}}^{d})^2}{V_{\mathcal{N}}^{d\,2}+V_{\mathcal{N}}^{q\,2}} & 0_{18x18} & 0_{18x18} & \mathbb{C}_q^{-1}(-(\mathbb{I}_3\otimes A_{\mathcal{N}})) \\ \mathbb{L}_0^{-1}((\mathbb{I}_3\otimes A_{\mathcal{N}}^T)) & 0_{18x18} & 0_{18x18} & \mathbb{L}_0^{-1}(-\mathbb{R}_0-\mathbb{L}_0\cdot(\mathbb{B}_0\otimes\mathbb{I}_{\mathcal{E}})) & 0_{18x18} & 0_{18x18} \\ 0_{18x18} & \mathbb{L}_d^{-1}((\mathbb{I}_3\otimes A_{\mathcal{N}}^T)) & 0_{18x18} & 0_{18x18} & \mathbb{L}_d^{-1}(-\mathbb{R}_d-\mathbb{L}_d\cdot(\mathbb{B}_d\otimes\mathbb{I}_{\mathcal{E}})) & 0_{18x18} \\ 0_{18x18} & 0_{18x18} & \mathbb{L}_q^{-1}((\mathbb{I}_3\otimes A_{\mathcal{N}}^T)) & 0_{18x18} & 0_{18x18} & \mathbb{L}_d^{-1}(-\mathbb{R}_d-\mathbb{L}_d\cdot(\mathbb{B}_d\otimes\mathbb{I}_{\mathcal{E}})) \end{bmatrix} \tag{B.10}$$

$$A_{12} = \begin{bmatrix} 0_{18x5} & 0_{18x5} \\ \mathbb{C}_d^{-1}\left(Diag\left(\frac{-V_{\mathcal{N}}^{d}}{V_{\mathcal{N}}^{d\,2}+V_{\mathcal{N}}^{q\,2}}\right)M_{conv}^T\right) & \mathbb{C}_d^{-1}\left(Diag\left(\frac{V_{\mathcal{N}}^{q}}{V_{\mathcal{N}}^{d\,2}+V_{\mathcal{N}}^{q\,2}}\right)M_{conv}^T\right) \\ \mathbb{C}_q^{-1}\left(Diag\left(\frac{V_{\mathcal{N}}^{q}}{V_{\mathcal{N}}^{d\,2}+V_{\mathcal{N}}^{q\,2}}\right)M_{conv}^T\right) & \mathbb{C}_q^{-1}\left(Diag\left(\frac{-V_{\mathcal{N}}^{d}}{V_{\mathcal{N}}^{d\,2}+V_{\mathcal{N}}^{q\,2}}\right)M_{conv}^T\right) \\ 0_{18x5} & 0_{18x5} \\ 0_{18x5} & 0_{18x5} \\ 0_{18x5} & 0_{18x5} \end{bmatrix} \quad A_{21} = \begin{bmatrix} 0_{5x18} & 0_{5x18} & 0_{5x18} & 0_{5x18} & 0_{5x18} & 0_{5x18} \\ 0_{5x18} & 0_{5x18} & 0_{5x18} & 0_{5x18} & 0_{5x18} & 0_{5x18} \end{bmatrix} \tag{B.11}$$

$$A_{22} = \begin{bmatrix} Diag\left(\frac{-1}{\tau_P}\right) & 0_{5x5} \\ 0_{5x5} & Diag\left(\frac{-1}{\tau_Q}\right) \end{bmatrix} \quad M_{conv} = \begin{bmatrix} 0&0&0&0&0&0&0&0&0&0&1&0&0&0&0&0&0&0 \\ 0&0&0&0&0&0&0&0&0&0&0&0&1&0&0&0&0&0 \\ 0&0&0&0&0&0&0&0&0&0&0&0&0&1&0&0&0&0 \\ 0&0&0&0&0&0&0&0&0&0&0&0&0&0&0&0&1&0 \\ 0&0&0&0&0&0&0&0&0&0&0&0&0&0&0&0&0&1 \end{bmatrix} \tag{B.12}$$

Bibliography

[1] A. Bidram and A. Davoudi, "Hierarchical structure of microgrids control system," *IEEE Transactions on Smart Grid*, vol. 3, no. 4, pp. 1963–1976, Dec 2012.

[2] L. Meng, M. Savaghebi, F. Andrade, J. C. Vasquez, J. M. Guerrero, and M. Graells, "Microgrid central controller development and hierarchical control implementation in the intelligent microgrid lab of aalborg university," in *2015 IEEE Applied Power Electronics Conference and Exposition (APEC)*. IEEE, 2015, pp. 2585–2592.

[3] L. Viswanathan and S. KUMAR, "A review: Control strategies for power quality improvement in microgrid," *International Journal of Renewable Energy Research (IJRER)*, vol. 8, no. 1, pp. 150–165, 2018.

[4] J. J. Justo, F. Mwasilu, J. Lee, and J.-W. Jung, "Ac-microgrids versus dc-microgrids with distributed energy resources: A review," *Renewable and Sustainable Energy Reviews*, vol. 24, pp. 387–405, 2013.

[5] M. E. Samper and R. A. Reta, "Regulatory analysis of distributed generation installed by distribution utilities," *IEEE Latin America Transactions*, vol. 13, no. 3, pp. 665–672, 2015.

[6] R. Lasseter, A. Akhil, C. Marnay, J. Stephens, J. Dagle, R. Guttromson, A. S. Meliopoulous, R. Yinger, and J. Eto, "Integration of distributed energy resources. the certs microgrid concept," 2002.

[7] Z. Fan, P. Kulkarni, S. Gormus, C. Efthymiou, G. Kalogridis, M. Sooriyabandara, Z. Zhu, S. Lambotharan, and W. H. Chin, "Smart grid communications: Overview of research challenges, solutions, and standardization activities," *IEEE Communications Surveys & Tutorials*, vol. 15, no. 1, pp. 21–38, 2013.

[8] C. L. T. Rodríguez, "Concepción de controladores reconfigurables para microinversores fotovoltaicos operando como unidades autónomas de generación de energía en microrredes," Ph.D. dissertation, 2012.

[9] A. Engler, O. Osika, M. Barnes, N. Jenkins, and A. Arulampalam, "Db1 local micro source controller strategies and algorithms," *Eur. Comm.*, 2004.

[10] T.-F. Wu, Y.-K. Chen, and Y.-H. Huang, "3c strategy for inverters in parallel operation achieving an equal current distribution," *IEEE Transactions on Industrial Electronics*, vol. 47, no. 2, pp. 273–281, 2000.

[11] J. M. Guerrero, L. G. De Vicuna, J. Matas, M. Castilla, and J. Miret, "A wireless controller to enhance dynamic performance of parallel inverters in distributed generation systems," *IEEE Transactions on power electronics*, vol. 19, no. 5, pp. 1205–1213, 2004.

[12] W. R. Issa, "Improved control strategies for droop-controlled inverter-based microgrid," *Doctoral Theses University of Exeter*, 2015.

[13] J. A. M. Rodríguez, "Operación y control de micro-redes operando en modo aislado," Ph.D. dissertation, Universidad Tecnológica de Pereira. Facultad de Ingenierías Eléctrica , 2015.

[14] K. Yu, Q. Ai, S. Wang, J. Ni, and T. Lv, "Analysis and optimization of droop controller for microgrid system based on small-signal dynamic model." *IEEE Trans. Smart Grid*, vol. 7, no. 2, pp. 695–705, 2016.

[15] A. A. A. Radwan and Y. A.-R. I. Mohamed, "Modeling, analysis, and stabilization of converter-fed ac microgrids with high penetration of converter-interfaced loads." *IEEE Trans. Smart Grid*, vol. 3, no. 3, pp. 1213–1225, 2012.

[16] P. A. Mendoza-Araya and G. Venkataramanan, "Impedance matching based stability criteria for ac microgrids," in *Energy Conversion Congress and Exposition (ECCE), 2014 IEEE*. IEEE, 2014, pp. 1558–1565.

[17] D. Karimipour and F. R. Salmasi, "Stability analysis of ac microgrids with constant power loads based on popov's absolute stability criterion," *IEEE Transactions on Circuits and Systems II: Express Briefs*, vol. 62, no. 7, pp. 696–700, 2015.

[18] P. Kundur, J. Paserba, V. Ajjarapu, G. Andersson, A. Bose, C. Canizares, N. Hatziargyriou, D. Hill, A. Stankovic, C. Taylor *et al.*, "Definition and classification of power

system stability," *IEEE transactions on Power Systems*, vol. 19, no. 2, pp. 1387–1401, 2004.

[19] R. Majumder, "Some aspects of stability in microgrids," *IEEE Transactions on power systems*, vol. 28, no. 3, pp. 3243–3252, 2013.

[20] Z. Shuai, Y. Sun, Z. J. Shen, W. Tian, C. Tu, Y. Li, and X. Yin, "Microgrid stability: Classification and a review," *Renewable and Sustainable Energy Reviews*, vol. 58, pp. 167–179, 2016.

[21] V. Mariani, F. Vasca, J. C. Vásquez, and J. M. Guerrero, "Model order reductions for stability analysis of islanded microgrids with droop control," *IEEE Transactions on Industrial Electronics*, vol. 62, no. 7, pp. 4344–4354, 2015.

[22] Z. Zeng, H. Yang, and R. Zhao, "Study on small signal stability of microgrids: A review and a new approach," *Renewable and Sustainable Energy Reviews*, vol. 15, no. 9, pp. 4818–4828, 2011.

[23] Z. Shuai, Y. Sun, Z. J. Shen, W. Tian, C. Tu, Y. Li, and X. Yin, "Microgrid stability: Classification and a review," *Renewable and Sustainable Energy Reviews*, vol. 58, pp. 167–179, 2016.

[24] S. D'Arco, J. A. Suul, and O. B. Fosso, "Control system tuning and stability analysis of virtual synchronous machines," in *Energy Conversion Congress and Exposition (ECCE), 2013 IEEE*. IEEE, 2013, pp. 2664–2671.

[25] N. Mohan and T. M. Undeland, *Power electronics: converters, applications, and design*. John Wiley & Sons, 2007.

[26] S. DArco, J. A. Suul, and O. B. Fosso, "A virtual synchronous machine implementation for distributed control of power converters in smartgrids," *Electric Power Systems Research*, vol. 122, pp. 180–197, 2015.

[27] J. Rocabert, A. Luna, F. Blaabjerg, and P. Rodriguez, "Control of power converters in ac microgrids," *IEEE transactions on power electronics*, vol. 27, no. 11, pp. 4734–4749, 2012.

[28] R. Teodorescu, M. Liserre, and P. Rodriguez, *Grid converters for photovoltaic and wind power systems*. John Wiley and Sons, 2011, vol. 29.

[29] H. Akagi, E. H. Watanabe, and M. Aredes, *Instantaneous power theory and applications to power conditioning*. John Wiley & Sons, 2017, vol. 62.

[30] J. A. Suul, K. Ljokelsoy, and T. Undeland, "Design, tuning and testing of a flexible pll for grid synchronization of three-phase power converters," in *Power Electronics and Applications, 2009. EPE'09. 13th European Conference on*. IEEE, 2009, pp. 1–10.

[31] O. D. Montoya, W. Gil-González, A. Garcés, and G. Espinosa-Pérez, "Indirect ida-pbc for active and reactive power support in distribution networks using smes systems with pwm-csc," *Journal of Energy Storage*, vol. 17, pp. 261–271, 2018.

[32] C. A. H. Mora, N. L. D. Aldana, and C. L. T. Rodríguez, "Diseño e implementación de controladores lineales para regulación del bus dc en convertidores vsc para hvdc," *Tecnura: Tecnología y Cultura Afirmando el Conocimiento*, vol. 18, no. 40, pp. 48–61, 2014.

[33] C. Bajracharya, "Control of vsc-hvdc for wind power," Master's thesis, Institutt for elkraftteknikk, NTNU, 2008.

[34] C. Bajracharya, M. Molinas, J. A. Suul, T. M. Undeland *et al.*, "Understanding of tuning techniques of converter controllers for vsc-hvdc," in *Nordic Workshop on Power and Industrial Electronics (NORPIE/2008), June 9-11, 2008, Espoo, Finland*. Helsinki University of Technology, 2008.

[35] V. Yaramasu, M. Rivera, B. Wu, and J. Rodriguez, "Predictive control of four-leg power converters," pp. 121–125, 2015.

[36] H. Akagi, E. Watanabe, and M. Aredes, *Instantaneous power theory and applications to power conditioning*, ser. 10. John Wiley and Sons, Inc., Hoboken, New Jersey: IEEE press series on power engineering, 2007.

[37] J. A. P. Lopes, A. G. Madureira, and C. C. L. M. Moreira, "A view of microgrids," *Wiley Interdisciplinary Reviews: Energy and Environment*, vol. 2, no. 1, pp. 86–103, 2013. [Online]. Available: https://onlinelibrary.wiley.com/doi/abs/10.1002/wene.34

[38] A. Hirsch, Y. Parag, and J. Guerrero, "Microgrids: A review of technologies, key drivers, and outstanding issues," *Renewable and Sustainable Energy Reviews*, vol. 90, pp. 402 – 411, 2018. [Online]. Available: http://www.sciencedirect.com/science/article/pii/S136403211830128X

[39] J. Schiffer, D. Zonetti, R. Ortega, A. M. Stankovi, T. Sezi, and J. Raisch, "A survey on modeling of microgridsfrom fundamental physics to phasors and voltage sources," *Automatica*, vol. 74, pp. 135 – 150, 2016. [Online]. Available: http://www.sciencedirect.com/science/article/pii/S0005109816303041

[40] Z. Miao, L. Piyasinghe, J. Khazaei, and L. Fan, "Dynamic phasor-based modeling of unbalanced radial distribution systems," *IEEE Transactions on Power Systems*, vol. 30, no. 6, pp. 3102–3109, Nov 2015.

[41] K. Rudion, Z. Styczynski, N. Hatziargyriou, S. Papathanassiou, K. Strunz, O. Ruhle, A. Orths, and B. Rozel, "Development of benchmarks for low and medium voltage distribution networks with high penetration of dispersed generation," *CIGRE Report*, 2006.

[42] G. W. Stagg and A. H. El-Abiad, *Computer methods in power systems analysis*, ser. McGraw-Hill series in electronic systems. McGraw-Hill, 1988, vol. 4.

[43] C. Zhang, "An introduction to averaging method," *Dynamics at the Horsetooth, online*, vol. 2, no. 676, 2010.

[44] Y. Gu, N. Bottrell, and T. C. Green, "Reduced-order models for representing converters in power system studies," *IEEE Transactions on Power Electronics*, vol. 33, no. 4, pp. 3644–3654, 2017.

[45] F. Capitanescu, "Critical review of recent advances and further developments needed in ac optimal power flow," *Electric Power Systems Research*, vol. 136, pp. 57 – 68, 2016. [Online]. Available: http://www.sciencedirect.com/science/article/pii/S0378779616300141

[46] M. E. Nassar, A. A. Hamad, M. Salama, and E. F. El-Saadany, "A novel load flow algorithm for islanded ac/dc hybrid microgrids," *IEEE Transactions on Smart Grid*, 2017.

[47] F. Hameed, M. Al Hosani, and H. Zeineldin, "A modified backward/forward sweep load flow method for islanded radial microgrids," *IEEE Transactions on Smart Grid*, 2017.

[48] G. C. Kryonidis, E. O. Kontis, A. I. Chrysochos, K. O. Oureilidis, C. S. Demoulias, and G. K. Papagiannis, "Power flow of islanded ac microgrids: Revisited," *IEEE Transactions on Smart Grid*, vol. 3053, pp. 4–6, 2018.

[49] G. Díaz, J. Gómez-Aleixandre, and J. Coto, "Direct backward/forward sweep algorithm for solving load power flows in ac droop-regulated microgrids," *IEEE Transactions on Smart Grid*, vol. 7, no. 5, pp. 2208–2217, 2016.

[50] Z. Kremens and M. Labuzek, "Load flow analysis incorporating frequency as a state vector variable," in *Harmonics and Quality of Power, 2000. Proceedings. Ninth International Conference on*, vol. 2. IEEE, 2000, pp. 526–530.

[51] C. Li, S. K. Chaudhary, M. Savaghebi, J. C. Vasquez, and J. M. Guerrero, "Power flow analysis for low-voltage ac and dc microgrids considering droop control and virtual impedance," *IEEE Transactions on Smart Grid*, vol. 8, no. 6, pp. 2754–2764, 2017.

[52] A. Eajal, M. A. Abdelwahed, E. El-Saadany, and K. Ponnambalam, "A unified approach to the power flow analysis of ac/dc hybrid microgrids," *IEEE Transactions on Sustainable Energy*, vol. 7, no. 3, pp. 1145–1158, 2016.

[53] A. A. Hamad, M. A. Azzouz, and E. F. El Saadany, "A sequential power flow algorithm for islanded hybrid ac/dc microgrids," *IEEE Transactions on Power Systems*, vol. 31, no. 5, pp. 3961–3970, 2016.

[54] H. Morais, P. Kádár, P. Faria, Z. A. Vale, and H. Khodr, "Optimal scheduling of a renewable micro-grid in an isolated load area using mixed-integer linear programming," *Renewable Energy*, vol. 35, no. 1, pp. 151–156, 2010.

[55] M. Uzunoglu, O. Onar, and M. Alam, "Modeling, control and simulation of a pv/fc/uc based hybrid power generation system for stand-alone applications," *Renewable energy*, vol. 34, no. 3, pp. 509–520, 2009.

[56] G. Kariniotakis, N. Soultanis, A. Tsouchnikas, S. Papathanasiou, and N. D. Hatziargyriou, "Dynamic modeling of microgrids," in *2005 International Conference on Future Power Systems*. IEEE, 2005, pp. 7–pp.

[57] I. Vokony and A. Dán, "Creation of stability index for micro grids," in *International Conference on Renewable Energies and Power Quality*. European Association for the Development of Renewable Energies, Environment , 2010, pp. 1–4.

[58] J. P. Lopes, C. Moreira, and F. Resende, "Control strategies for microgrids black start and islanded operation," *International journal of distributed energy resources*, vol. 1, no. 3, pp. 241–261, 2005.

[59] X. Li, Y.-J. Song, and S.-B. Han, "Frequency control in micro-grid power system combined with electrolyzer system and fuzzy pi controller," *Journal of Power Sources*, vol. 180, no. 1, pp. 468–475, 2008.

[60] F. Katiraei, M. Iravani, and P. Lehn, "Small-signal dynamic model of a micro-grid including conventional and electronically interfaced distributed resources," *IET generation, transmission & distribution*, vol. 1, no. 3, pp. 369–378, 2007.

[61] Z. XIAO, C. WANG, and S. WANG, "Small-signal stability analysis of microgrid containing multiple micro sources [j]," *Automation of Electric Power Systems*, vol. 6, p. 022, 2009.

[62] C.-T. Chen, *Linear system theory and design*. Oxford University Press, Inc., 1998.

[63] D. Mondal, A. Chakrabarti, and A. Sengupta, *Power system small signal stability analysis and control*. Academic Press, 2014.

[64] I. J. Pérez-Arriaga, G. C. Verghese, and F. C. Schweppe, "Selective modal analysis with applications to electric power systems, part i: Heuristic introduction," *ieee transactions on power apparatus and systems*, no. 9, pp. 3117–3125, 1982.

[65] G. Verghese, I. Perez-Arriaga, and F. Schweppe, "Selective modal analysis with applications to electric power systems, part ii: The dynamic stability problem," *IEEE Transactions on Power Apparatus and Systems*, no. 9, pp. 3126–3134, 1982.